Structural, Morphological, Dielectric and Impedance Study of Lithium Iron Phosphate ($LiFePO_4$)

A Project Work Submitted

In Partial Fulfilment of the Requirements for the

Degree of

MASTER OF SCIENCE

In

CHEMISTRY

by

ANKIT CHATURVEDI

(2k22/MSCCHE/60)

Under the Supervision of

Prof. Rajinder. K. Gupta

DR. Amrish K. Panwar

Department of Applied Chemistry and

Department of Applied Physics

DELHI TECHNOLOGICAL UNIVERSITY

(formerly Delhi College of Engineering)

Shahabad Daulatpur, Main Bawana Road, Delhi-110042, India

MAY, 2024

DELHI TECHNOLOGICAL UNIVERSITY

(formerly Delhi College of Engineering)

Shahbad Daulatpur, Main Bawana Road, Delhi-110042, India

CANDIDATE DECLARATION

I, **ANKIT CHATURVEDI (2k22/MSCCHE/60)** hereby certify that the work which is being presented in the dissertation enlightened "**Structural, Morphological, Dielectric and Impedance Study of Lithium Iron Phosphate ($LiFePO_4$)**" in partial fulfilment of the requirements for the award of the Degree of Master in Science, submitted in the Department of Applied Chemistry, Delhi Technological University is an authentic record of my own work carried out during the period from June 2023 to Mar 2024 under the supervision of Prof. **Rajinder. K. Gupta** and Dr. **Amrish K. Panwar**.

I declare that the content of this thesis is original and has not been previously submitted by me to fulfil the requirements for obtaining any degree from this or any other university or institution.

Place: Delhi **ANKIT CHATURVEDI**

Date: /05/2024 **(2k22/MSCCHE/60)**

DELHI TECHNOLOGICAL UNIVERSITY

(formerly Delhi College of Engineering)

Shahbad Daulatpur, Main Bawana Road, Delhi-110042, India

CERTIFICATE

Certified that Ankit Chaturvedi (2k22/MSCCHE/60) has carried out his research work presented in this dissertation entitled "Structural, Morphological, Dielectric and Impedance Study of Lithium Iron Phosphate ($LiFePO_4$)" for the award of Master of Science from the Department of Applied Chemistry, Delhi Technological University, Delhi, under our supervision. I affirm that this thesis represents the outcome of my own research and investigations. The work described herein was conducted independently by me, and the material presented does not form the foundation for the conferment of any other academic degree, either to me or to any other individual from this or any other educational institution.

PLACE: DELHI **Prof. Rajinder. K. Gupta**

Date: 30/05/2024 **(Supervisor)**

Dr. Amrish K. Panwar

(Co-Supervisor)

ACKNOWLEDGEMENT

The accomplishment of this project was greatly facilitated by guidance and assistance from many people and I felt very fortunate to have their assistance throughout its completion.

I would like to express my gratitude towards my project supervisor, Prof. Rajinder. K. Gupta, Department of Applied Chemistry, Delhi Technological University, and my Co-supervisor Dr Amrish K. Panwar, Applied Physics, Delhi Technological University, Delhi who provided me with a great opportunity to work under their competent guidance. Their scholarly and insightful advice enabled me to complete the project on schedule.

I also want to express my gratitude to Dr. Amrish K. Panwar for his valuable assistance and willingness to dedicate time to help me improve, which played a crucial role in the success and completion of my project.

I am grateful and fortunate enough to receive constant encouragement, support, and assistance from all the lab members of Mr. Sharad Singh Jadaun Sir and Mr. Naveen, research scholar, applied physics, DTU and the teaching staff of the Department of Applied Chemistry, which assist me in completing my project work.

Finally, yet importantly, I extend my sincere gratitude to my beloved family and friends who have supported me through my long working hours and whose encourage me to kept me going.

Ankit Chaturvedi

ABSTRACT

Lithium-ion batteries are getting more attention as prominent energy storage devices because of its high-power energy density and better cyclability compared to other energy storage devices. With the growing interest in developing rechargeable batteries, For the next generation of Li-ion batteries, lithium iron phosphate ($LiFePO_4$) is one of the potential cathode materials because of its more cyclic stability, environmental friendliness and economic viability. Here in this study, The $LiFePO_4$ cathode material has been synthesized using a solid-state reaction method using two-step heating under different calcination temperatures in a reduced inert atmosphere. Pre-heating results in decomposition and calcination at high temperatures leading to the crystallization of $LiFePO_4$. Primary $LiFePO_4$ was synthesized by preheating at 350 ^{0}C and calcinated at 750 ^{0}C. The structural, morphology, elemental distribution and Impedance with Dielectric study of synthesized pristine $LiFePO_4$ are carried out by X-ray powder diffraction (XRD), Field emission Scanning electron microscopy (FE-SEM), and electrochemical impedance spectroscopy (EIS), respectively. XRD result shows an orthorhombic olivine structure with a "Pnma" space group of LFP. The crystallite size of 36 nm and the strain in an atom of $8.6*10^{-4}$ has been observed as estimated from Scherrer's equation and W-H plot, respectively. The physical characterizations and the particle-size distribution data supported the aggregation and sintering observed by the SEM during the calcination process. The electrical properties and impedance are measured by impedance spectroscopy over the temperature range of 50 to 150 °C. It reveals the diffusion of Li^+ ion in pristine $LiFePO_4$. Dielectric analysis shows the charge storage capacity of $LiFePO_4$ concerning the variation of temperature and dielectric loss in pristine $LiFePO_4$ samples

Keywords: Li-ion battery, $LiFePO_4$, cathode material, orthorhombic, rate performance

CONTENTS

LIST OF FIGURES

List of table:

LIST OF ABBREVIATIONS AND SYMBOLS:

LIB: Lithium-ion battery

LFP: $LiFePO_4$

LMO: $LiMn_2O_4$

LCO**:** $LiCoO_2$

IEC: International electrotechnical commission

K: dimensionless shape factor (0.9)

θ: Bragg angle;

εr: dielectric constant

βt :FWHM of XRD peaks or half-height width of the XRD diffraction peak

CHAPTER 1:

INTRODUCTION AND LITERATURE REVIEW

1.1 INTRODUCTION

Utilising renewable energy sources to address the threat of global warming and the limited oil storage capacity has become one of the biggest problems in recent years. So nowadays, Li-ion battery is extensively used in electronic devices [1] due to their high long cycle life and high electron density. These are also a promising energy source for hybrid electric vehicles. Rechargeable batteries for vehicle applications still face challenges in designing and producing high-performance, high-safety, and affordable batteries. In the rapidly evolving field of energy materials, LIBs are the focus of substantial study and are widely used in consumer electronics, military, and aviation industries. In Li-ion batteries, the process of intercalating Li ions into anodes from cathodes through a nonaqueous electrolyte that contains Li ions is reversed during discharge [2]. In charged or discharged, lithium ions go back and forth between the anode and cathode; while electrons do the same via the external electrical circuit.

For Li-ion batteries battery life, cyclic life, cost, and safety are all significantly impacted by the cathode. If we compare layered lithium nickel-cobalt-manganese oxide $LiMO_2$ (M = Mn, Co, Ni), $LiCoO_2$ was used as the cathode material for commercial batteries [3] and spinel manganite ($LiMn_2O_4$), at high temperatures. $LiFePO_4$ exhibits a higher degree of structural stability when compared to layered oxide compounds such as $LiCoO_2$ and spinel type ($LiMn_2O_4$), rendering it more resistant to structural distortions or alterations. and spinel type ($LiMn_2O_4$), because both Fe and P atoms form strong bonds with the oxygen atoms. $LiFePO_4$ remains stable up to 400 °C, while $LiCoO_2$ begins to break down at 250 °C [4]. $LiFePO_4$ is a better cathode material. Padhi *et al.* in 1997 reported the electrochemical properties of $LiFePO_4$ [5]. The olivine phase $LiFePO_4$ is one of the most promising cathode materials because of its low weight, high safety, good cyclic stability, high energy density, good thermal stability, prolonged life span, environmental friendliness, low toxicity, relatively low cost, and with a voltage plateau around 3.4-3.5v vs Li/Li^+, the theoretical capacity of $LiFePO_4$ was observed around 170mAh/g [6,7]. Good cycle performance and operating safety are achieved by $LiFePO_4$ due to its strong lattice stability. However, low ionic diffusivity (10^{-11} to 10^{-13} cm^2 s^{-1}) and poor electronic conductivity ($\sim 10^{-9}$ cm s^{-1}) are also a result of the strong covalent oxygen bonding.

Hence to overcome these challenges of slow Lithium-ion diffusion of $LiFePO_4$ and low electronic conductivity, different techniques for doping of $LiFePO_4$ with supervalent cation, reduction of particle size, therefore coating with carbon-based material and morphological improvements were explored [8]. The preparation of $LiFePO_4$ involves several techniques, including spray pyrolysis, hydrothermal, microwave, sol-gel, high-temperature solid-phase, and carbothermal reduction methods.

Recently, cathode materials of class as NASICON or olivine polyoxyanion structures have been explored. These structures are constructed from MO6 octahedra (where M is Fe, Ti, V, or Nb) and XO_4^{n-} (where S, P, W, Mo) tetrahedral anions [8,12]. The orthorhombic unit cell (D^{16}_{2h}-space group Pnma) of phospho-olivine-type $LiFePO_4$ can hold four units of LiFePO4, and the lattice parameters of a, b and c are 0.6008, 1.0334 and 0.4693 nm, respectively [8,9]. The divalent Fe ions occupy corner-sharing octahedra, the P ions occupy tetrahedral sites with a distorted hexagonal close-packed framework, and the Li^+ ions are arranged in chains of edge-sharing octahedral [8,10]. The PO_4 tetrahedron and FeO_6 are not directly connected in the Centre of the octahedral structure The FeO_6 octahedron shares the edge with two LiO_6 octahedrons and a PO_4 tetrahedron. There is a formation of a one-dimensional tunnel by the edge-shared Li octahedra for the mobility of Li^+ ions in these tunnels [10,15].

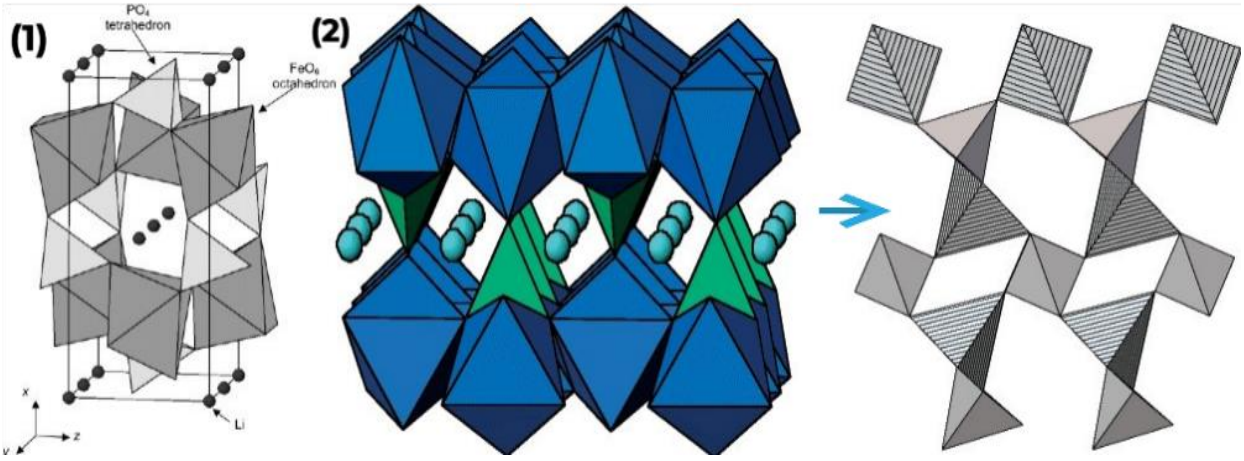

Fig. 2.1 Structure of $LiFePO_4$ [10]

Fig.1.3. Orthorhombic $LiFePO_4$ and Trigonal Quartz-like structure of $LiFePO_4$

As seen in Fig. 1, the olivine structure is most appropriate for the passage of lithium ions in the tunnels parallel to the [010] direction of the structure [10,15]. Lithium undergoes a two-phase reaction within the material. Transitioning between $LiFePO_4$ and $FePO_4$, which are structurally identical. $LiFePO_4$ primarily contains one Li-ion per formula unit. This Li-ion is transferred to the anode during the first charge phase to maintain the balance of oxidation of Fe^{2+} to Fe^{3+}. On the other hand, the elimination of lithium ions results in the formation of the $FePO_4$ phase. So $LiFePO_4$ is developed into $FePO_4$ shown in Fig. 2 [16,24].

$LiFePO_4$ is synthesized by High-temperature solid-phase, carbothermal reduction, sol-gel, microwave, spray pyrolysis, polyol process, hydrothermal, coprecipitation, and other synthesis processes are among the methods used [12,15,23,]. But $LiFePO_4$ can be prepared conventionally by solid-state synthesis Rakesh Saroha et al [12]. This approach is simple to follow and easy to industrialize. However, the synthesis process takes a lengthy time, and the final product has particles that are irregular and have a non-crystalline shape. Repeated grinding and calcination are necessary for the extended, complex processes, which result in the creation of bigger particles with poor electrochemical performance [13,17]. In general, CH_3COOLi, Li_2CO_3, $LiOH{\cdot}2H_2O$and LiF were used as the lithium source, $FePO_4(H_2O)_2$, Fe $(CH_3COO_2)_2$ and $FeC_2O_4{\cdot}2H_2O$ were used as the iron source, $NH_4H_2PO_4$ and $(NH4)_2HPO_4$ were used as the phosphorus source [24]. The characteristics of $LiFePO_4$ are significantly affected by the sintering temperature, which affects both the material discharge capacity and the purity of the $LiFePO_4$ particles [19,22]. Therefore, it is crucial to select a moderate temperature. In general, the range of 650–700 °C is ideal for sintering [20].

In this research paper, we have synthesized the $LiFePO_4$ sample using the solid-state reaction method and investigated its structural, morphological, dielectric and electrical properties. The phase and purity of the LFP were confirmed by XRD analysis at room temperature. Crystal size and elemental distribution were analyzed by FE-SEM. We carefully studied the impedance spectra to understand the electrical and dielectric properties of $LiFePO_4$ pellets. By analyzing the Impedance data; we can identify different electrical components, polarization, permittivity and relaxation effects in the material.

1.2Literature Review:

1.2.1 BATTERY

Battery is an electrochemical device, a battery uses chemical reactions to store and produce electrical energy. A battery consists of one or more electrochemical units, referred to as cells, wherein each cell comprises an electrolyte solution and two electrodes, namely a positive electrode (cathode) and a negative electrode (anode). A battery's basic mechanism is the flow of electrons via an external circuit to produce electrical power and the movement of ions between the electrodes through the electrolyte.[21]

There are 5 key components in battery

Anode, Cathode**,** Electrolyte, Separator, Current Collectors

Anode: The negative electrode during discharge, where oxidation occurs (loss of electrons). It releases electrons to the external circuit and ions to the electrolyte.

Cathode: During the discharge process, the positive electrode (cathode) functions as the oxidizing agent, facilitating the flow of electrons from the external circuit, where reduction occurs (gain of electrons). It receives electrons from the external circuit and ions from the electrolyte.

Electrolyte: A medium that allows the flow of ions between the anode and cathode but is non-conductive to electrons. It can be a liquid, gel, or solid.

Separator: A physical barrier that separates the anode and cathode to prevent short-circuiting while allowing ion flow.

Current Collectors: Materials that conductively link the electrodes to the external circuit , typically made of metals like copper (for the anode) and aluminium (for the cathode).

On basis of working batteries are of two types:

1.2.1.1 PRIMARY BATTERY

Batteries referred to as primary batteries or non-rechargeable batteries are designed for single-use, where their chemical reactions are not reversible, and they cannot be recharged after being fully discharged, are often overshadowed by secondary or rechargeable batteries in the media. A strong focus on one product over another can lead people to believe that primary batteries are old technology on their way out. Not like that. Primaries are essential in scenarios when charging is impractical or impossible, for as in military warfare, rescue operations, and forest fire services. The IEC 60086-regulated main batteries are also utilized to power various devices such as smart meters, animal trackers, remote light beacons, wristwatches, electronic keys, cardiac pacemakers, tire pressure monitors, and smart meters. Compared to other power

sources, primary batteries are significantly more advantageous because of their high specific energy, long store lives, and immediate readiness. They may be transported to distant locations and utilized immediately, even after prolonged storage. [22]

Specific energy does not account for power delivery, which is a flaw in the majority of main batteries; rather, it solely represents a battery's carrying capacity. Primary battery manufacturers rarely provide exact power; instead, they often publish specified energy. Consumer-grade primary batteries have their capacity assessed at a very low current of 25mA, however For the majority of rechargeable (secondary) battery systems, their rated capacity is determined based on a discharge rate of 1C, which corresponds to a current that would fully discharge the battery in one hour under standard conditions. Furthermore, before being considered entirely discharged, the batteries are permitted to drop from the nominal 1.5V for alkaline to 0.8V. [23] On paper, this gives impressive readings, but when applying loads with higher current draws, the results are not as pleasing.

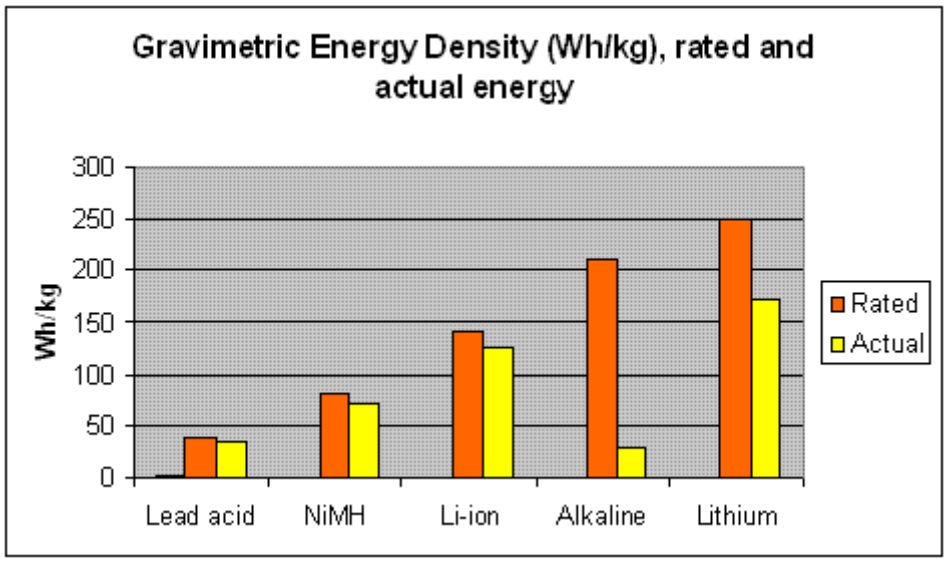

Figure 1.3: Energy comparison underload.

evaluates primary and secondary battery performance as "Rated" and "Actual." Most secondary batteries are rated for actual discharges at 1C, which corresponds to the specific energy while discharging at a relatively low current. The diagram amply illustrates how the lead acid, NiMH, and Li-ion secondary batteries have lower rated capacities (Rated) but function better when loaded to a 1C discharge (Actual), whereas the primary alkaline batteries work well with light loads characteristic of entertainment devices. The high internal resistance of primary batteries

contributes to low performance under load conditions by causing the voltage to collapse. Ohms (Ω) are used to measure resistance, which controls how easily electrical current passes through a substance or object. The already high resistance rises even greater during discharge as the battery runs out of power. A power tool on an alkaline battery would be unfeasible for digital cameras with primary batteries, which are borderline circumstances. Usually, a digital camera's used alkaline battery can last the kitchen clock for two years. [3,17]

1.2.1.2 SECONDARY BATTERY

The most common rechargeable battery types are **lead acid, NiCd, NiMH,** and **Li-ion**. These are a quick review of their features. Rechargeable batteries are essential to our everyday life; many tasks would be impossible without the ability to recharge them.[25]

- First type of rechargeable battery is **lead acid**. Although lead acid is inexpensive, durable, and forgiving if misused, its specific energy is low and its cycle count is restricted.

Wheelchairs, golf vehicles, personnel carriages, emergency lights, and uninterruptible power supplies (UPS) are among the items that employ lead acid. Lead cannot be disposed of in landfills because it is hazardous.

- **Cadmium and nickel NiCd** is a mature and well-understood metal that finds application in situations requiring high discharge current, long service life, and harsh temperatures. NiCd batteries are among the strongest and longest-lasting because they are the only ones that can charge very quickly under pressure. Aircraft, power tools, UPSs, and medical equipment are the main applications. because to environmental concerns, nickel-cadmium is being replaced by alternative compounds; nonetheless, because to its excellent safety record, airplanes continue to use nickel-cadmium.

- **Nickel-metal-hydride** – acts as a substitute for nickel since it has a greater specific energy and only contains mildly hazardous elements. NiMH is utilized in industrial applications, hybrid automobiles, and medical devices. NiMH is also offered to consumers in AA and AAA cell sizes.

- **Lithium-ion batteries** are taking the place of lead and nickel-based batteries in numerous applications. A protective circuit is required for Li-ion because of safety concerns. Although it

costs more than most other batteries, the cost per cycle is lower than with many other chemistries thanks to its high cycle count and low maintenance. [26]

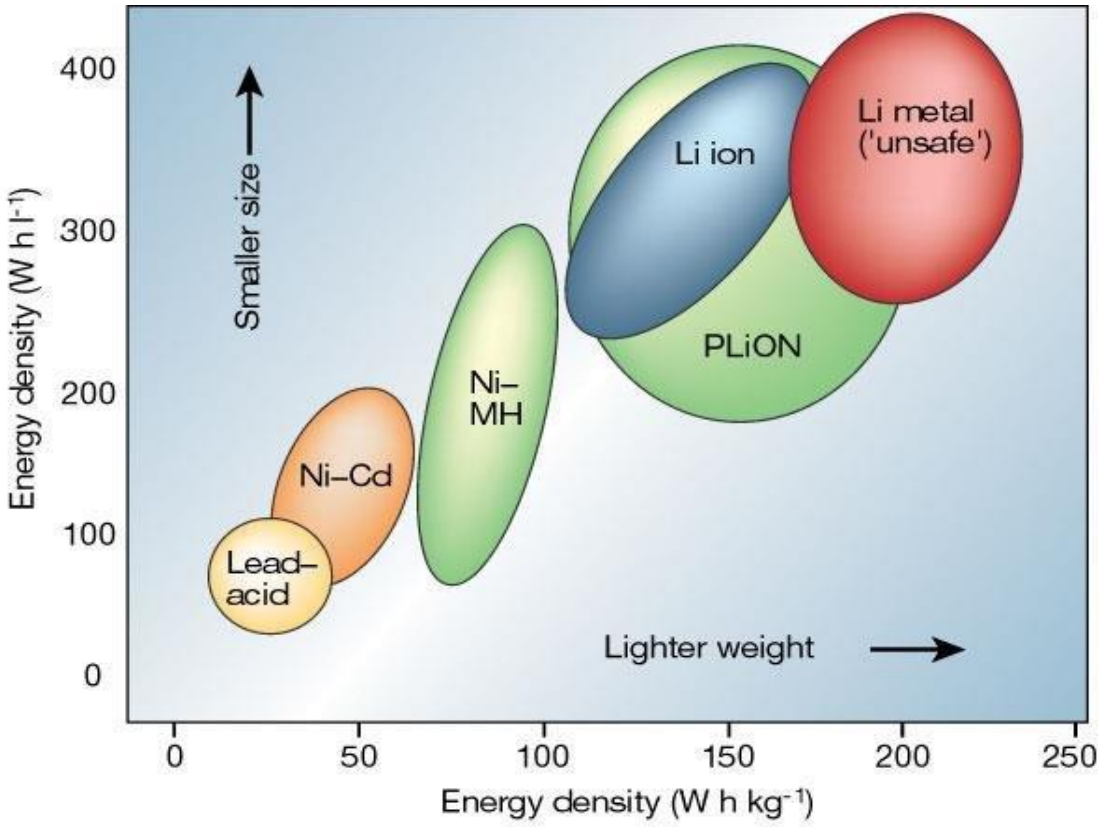

Figure 1.4: Specific energy comparison of secondary and primary batteries

1.2.2 CATHODE

Electricity is produced by the chemical reactions of Lithium in a Lithium-ion battery. This is the rationale behind the addition of sodium to the battery; the area designated for this purpose is known as the "cathode." Lithium metal oxide is utilised as the cathode.[27] active material containing lithium ion, and conductivity is enhanced by incorporation of the conductive addition; additionally, the binder act as an adhesive to facilitate the proper settling of conductive additive and active material settle on the aluminium substrate.[28] An essential factor in defining the battery's properties is the cathode. since the type of active material utilised for the cathode determines the battery's voltage and capacity. As the lithium ion concentration increase with increase in the capacity, while the voltage increases with greater potential

difference between cathode and anode. Anode have small potential difference depending on their type, while cathodes shows significant difference. consequently, batteries voltage greate influence by the cathode.[27]

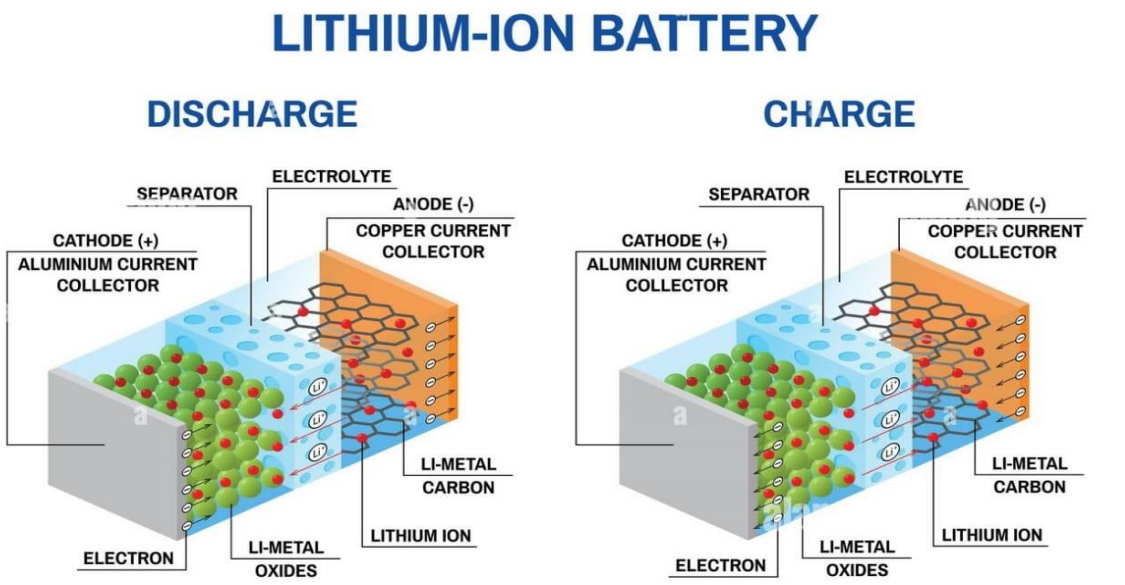

Figure 1.5: diagram of the charging and discharging process of Li-ion battery

cathode act as positive electrode. In Li-ion batteries, the process of intercalating Li ions into anodes from cathodes through a nonaqueous electrolyte that contains Li ions is reversed during discharge [2]. In charged or discharged, lithium ions go back and forth between the anode and cathode; while electrons do the same via the external electrical circuit.

The most common cathode materials are Layered ($LiCoO_2$), Spinal (Li-Mn-O), olivine ($LiFePO_4$) and Tavorite ($LiFe(SO_4)F$).

1.2.2.1 Lithium metal oxides ($LiMO_2$)

The formula for the layered lithium transition metal oxide is $LiMO_2$, a cathode material category that includes M=Co, Mn, Ni, or a combination of two or more, which has certainly proven to be the most successful for LIBs. Their layers of structure provides an abundance of

diffusion pathways for lithium ions, which is responsible for their outstanding electrochemical performance. Fast charging and discharging applications are ideal for layered metal oxides. When exposed to temperatures over 300 °C, these materials seem to be performing well. [29]

Limitation: Lithium manganese oxide cathode materials face challenges like capacity loss by manganese dissolution, structural damage, limited cycling life, and lower energy density. Researchers are exploring solutions such as doping, coatings, and electrolyte optimization

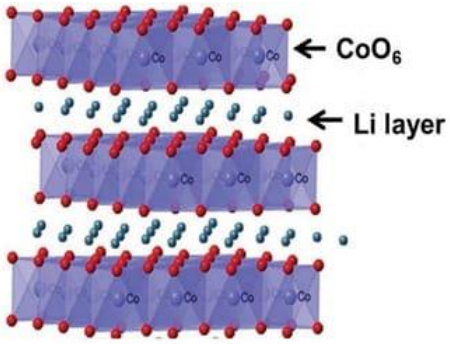

Fig 1.6: Crystal structure of $LiCoO_2$.

1.2.2.2. Spinel Lithium Transition Metal Oxides ($LiMn_2O_4$)

The compound Li-Mn-O has a long history of research dating back centuries, making it one of the oldest compounds studied. It continues to be widely used today for its initial purpose as a depolarizer. Li-Mn-O is valued for its easy accessibility, environmentally friendly, low cost, and favourable electrochemical properties. Li-Mn-o spinels have many advantages, including high thermal resistance, good performance, and safety for health and the environment. The diffusion rate at which Li^+ ions move in this material is between 10^{-6} and 10^{-10} sq. cm/s.[30]

Limitations: The capacity of lithium manganese oxide cathodes decreases with frequent cycling due to the instability of Mn^{3+} ions, especially above 55°C. This causes manganese to dissolve, reducing capacity and impacting battery performance and lifespan. Maintaining stable conditions and adjusting operational settings are essential to improve cycling stability.

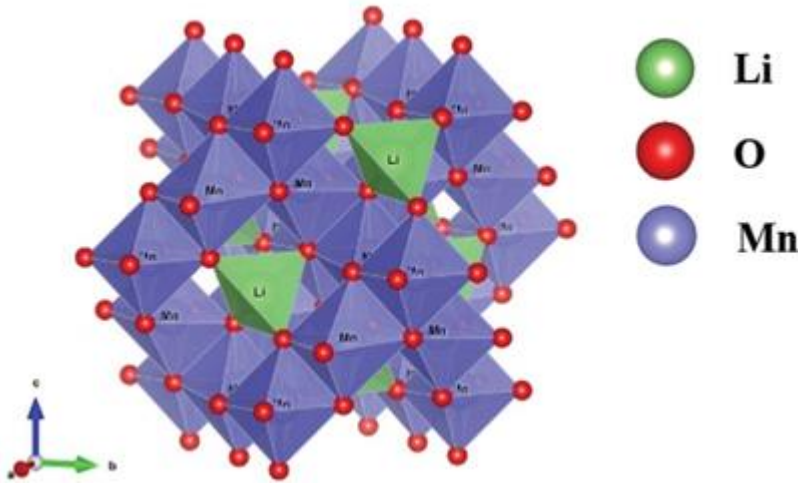

Fig. 1.7: crystal structure of $LiMn_2O_4$

1.2.2.3. Olivine Lithium Metal Phosphates and Silicates ($LiMPO_4$ and $LiMSiO_4$)

These compounds are often called $LiFePO_4$. They have a steady discharge level and a moderate capacity of about 150-160 mAh/g. [5,15, 22] $LiFePO_4$ is less hazardous, inexpensive, non-toxic, and has excellent chemical and thermal stability. It also loses less capacity with time. They have less volume changes and heat generation during charging compared to other materials. This makes them safer than Li-cobalt cathodes for advanced uses. Compared to other cathode materials, olivine-structured compounds have several benefits, such as a material structure that is barely altered by the intercalation and deintercalation of lithium ions. It has a high voltage system of approx. 4V.

Limitations: The main limitations of olivine LFP cathodes are low electrochemical performance by slow lithium-ion diffusion rate due to the 1D motion of Li-ion and poor electronic conductivity by hindering the electron flow during charging and discharging. Two methods are developed to improve this challenge. One involves the reduction of cathode particles and the second is to use nanocomposite of $LiFePO_4$ with conductive carbon matrix[13]

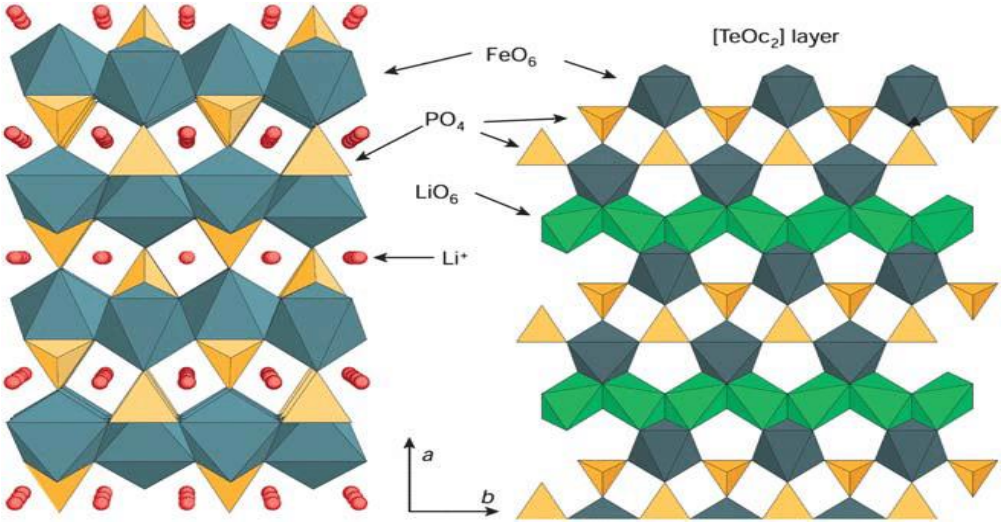

Fig 1.8: Crystal structure of olivine $LiFePO_4$

1.2.2.4. Tavorite $LiM(TO_4)X$

Tavorite is categorise as the material with general formula $LiM(TO_4)X$. A is usually an alkali or alkaline-earth element, M is a metal, T is a p-block element, and X is O, OH, or F. In lithium iron fluorophosphate, a single Li^+ ion can be cycled through charge and discharge process with the theoretical capacity of 153 mAh/g.[31] $LiFePO_4$ F is one of the best tavorite structures. Tavorite structure is similar to olivine but different in some properties. It shows good thermal stability, cost-effective, environmentally friendly, higher rate capacity and faster Li-ion diffusion compared to LFP. Tavorite LFP often contains fluorine ($LiFePO_4F$), which may be introduced during synthesis. Fluorine raises concerns about long-term stability, safety, and environmental impact.

Tavorite structures confidently exhibit one-dimensional diffusion channels with low activation energies.Their property enables fast charging and discharging of compounds such $Fe(SO_4)F$ and $V(PO_4)F$. These findings imply that cathode materials with tavorite structures are better options for enhancing next lithium-ion batteries. [32]

Limitations: Tavorite is a phase which is metastable state and can readily transfer into the olivine phase. pure tavorite LFP is more difficult compared to olivine LFP. So large scal production of tavorite no possible like olivine. Tavorite is thermally stable but these are affected

at extreme temperature. F can potentially react with the electrolyte or other cell components, leading to degradation or safety issues so Structure degradation over the repeated cycle occur result in performance loss.[32]

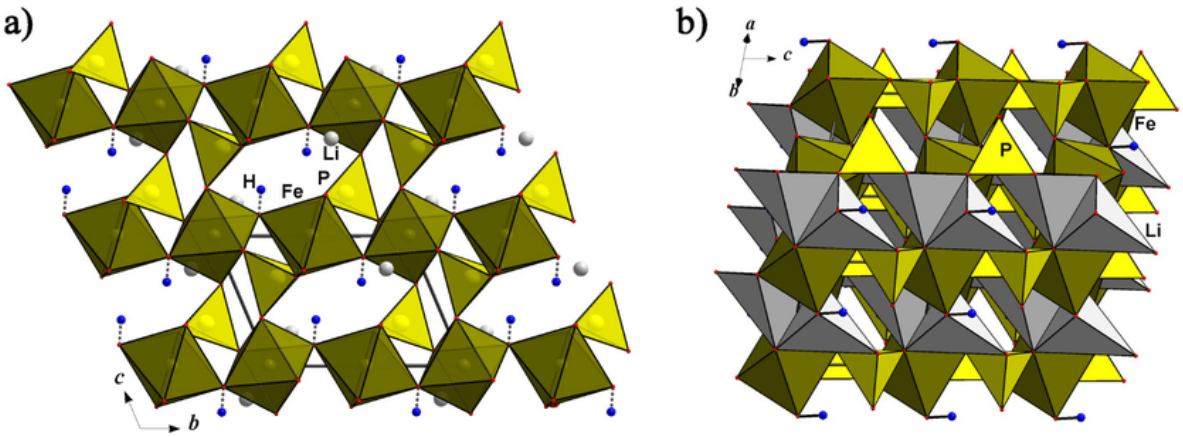

Fig 1.9: Crystal structure of tavorite $LiFePO_4F$

CHAPTER 2:

MATERIAL AND SYNTHESIS

2.1 Synthesis of $LiFePO_4$

$LiFePO_4$ was prepared by reacting $CH_3COOLi{\cdot}2H_2O$ (99%), $FeC_2O_4{\cdot}2H_2O$ (99%) and $(NH_4)_2HPO_4$ (99.5%) in stoichiometric proportions through solid-state reaction without the addition of carbon additives as the conducting material. To keep the iron from oxidation, the synthesis of $LiFePO_4$ was attempted through two-step heating under inert Ar flow. A reduced atmosphere (90% Ar+10% H_2) is required for the conversion of Fe^{+3} into Fe^{+2} and a high temperature is required to form the crystalline phase $LiFePO_4$ [14,25]. The mixture was ground together into a paste with acetone in an agate mortar. The resultant material was separated into two portions, each of which was pre-heated at two different temperatures viz. 300 °C and 350 °C for 5 h in Ar/H_2 (90:10 v%) in a tubular furnace to form the $LiFePO_4$ precursor, So it decomposes at 300 °C and 350 °C. Subsequently, heated samples were ground again for 2 h and calcinated at 700 °C and 750 °C for 12 h. Decomposing and calcination were both carried out in a 90% Ar + 10% H_2 atmosphere. All heating and cooling rates of Ar/H_2 (90:10 v%) were at 2 °Cmin^{-1} in a tubular furnace. The pellets were formed at 700 °C in Ar/H_2 (90:10 v%) in a tubular furnace for 10 h for the study of EIS spectra.

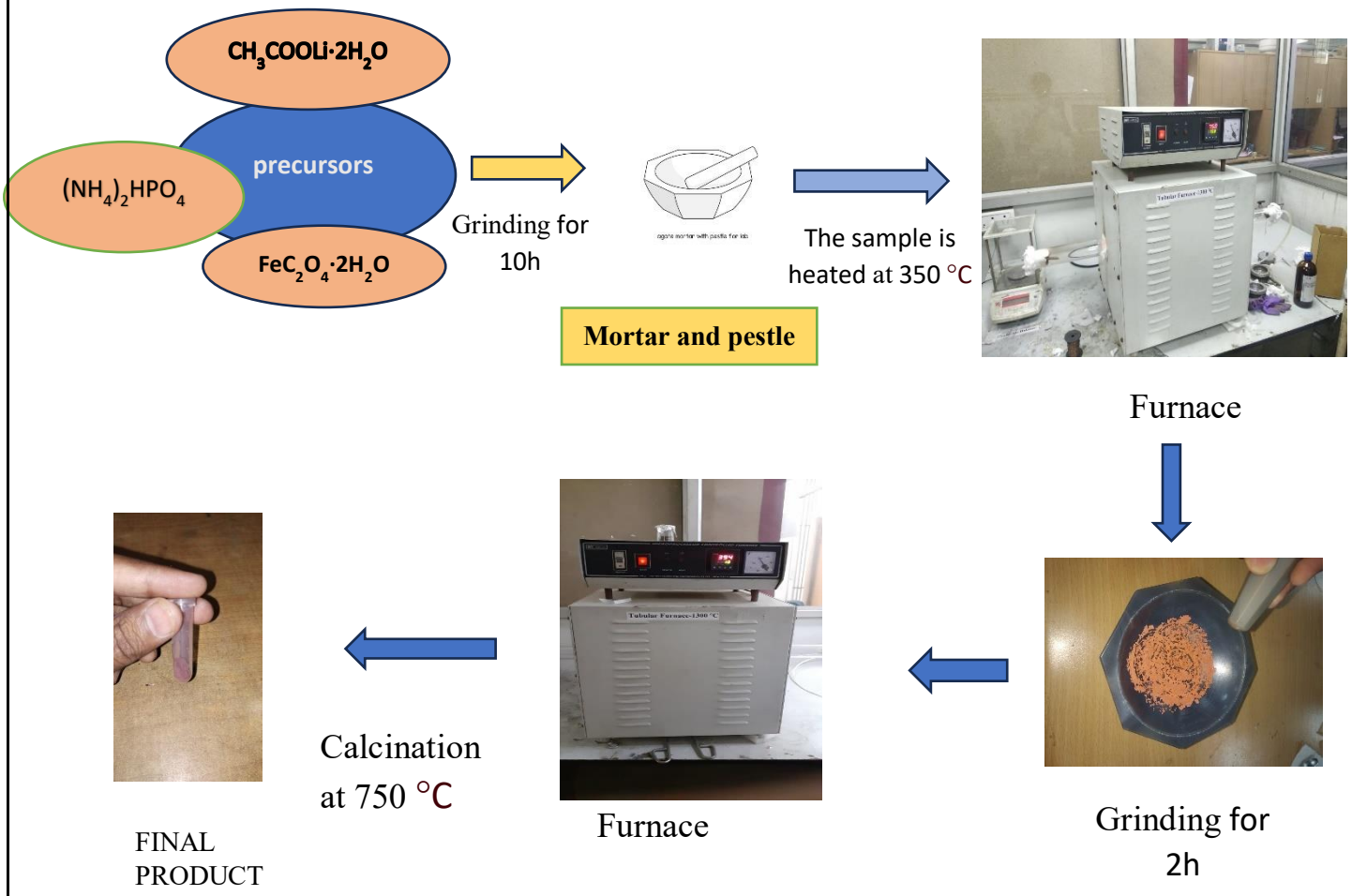

Fig 2.1: The synthesis of $LiFePO_4$ through solid-state reaction under reducing inert atmosphere(Ar/H_2 (90:10 v%))

2.2 Material characterization

Powder X-ray diffraction (XRD) with Cu_Kα radiation was carried to determine the crystalline structure and phase purity of LiFePO4. (λ=1.54178 Å) using a Philips PW 1840 X-ray diffractometer at 36 kV, 20 mA. A wide 2θ XRD measurement range from 10° to 60° has been used to obtain the diffracted data of the synthesized materials at a scanning rate of 5°min-1. The morphological properties were observed by combining Field Emission Scanning Electron Microscopy (FE-SEM) with energy-dispersive X-ray (EDX). EDX is used to analyse the elemental composition on solid surfaces at different morphologies. Cathode-electrolyte interface's charge transfer resistance and dielectric study can be determined using the EIS measurement within the frequency range of 4 Hz–8 MHz.

Figure 2.2: Different synthesis techniques utilized to produce cathode materials.

2.3 Synthesis methods

Different ways to make $LiFePO_4$ are being studied to make it work better. Some of these methods are solid-state reaction, sol-gel process, microwave techniques, hydrothermal synthesis, carbothermal reduction, spray pyrolysis, and more.

2.3.1 Solid state method:

The solid-state method is commonly used to make various materials in materials science, including ceramics, metals, and alloys. In lithium-ion battery technology, this method is often used to produce compounds like lithium manganese phosphate ($LiMnPO_4$) and lithium iron phosphate ($LiFePO_4$). It is simple and can be used in large-scale production. The initial product has uneven particles, no crystal structure, and takes a long time to make. The complex steps include grinding and heating repeatedly, which makes the particles bigger but less effective in batteries.[15,22, 25]

In order to complete this process, the precursors must be measured out and ground in an agate mortar. After that, the powder is heated for a few hours at 350 to 400°C in a crucible or porcelain basket. This step decomposes the initial ingredients and eliminates volatile substances like NH3, NO2, CO2, and H2O, leaving only the oxides behind. The mixture is ground again after being removed from the oven to enhance uniformity and reduce grain size.[33]

2.3.2 Sol-gel method

The sol-gel process creates solid materials from small molecules, often used to make metal oxides like silicon and titanium oxides. Monomers in a solution become a colloidal solution (sol), which forms a network (gel) of particles or polymers. This method helps control reactions in solid synthesis. It makes it easier to create consistent multi-component systems, especially uniform mixed oxides made by mixing precursor solutions. The process is simple and can be done at low temperatures with basic equipment. However, it can be difficult to scale up for large-scale production.

The hydrolysis of the precursor in acidic or basic media and the polycondensation of the hydrolysed products are the two primary reactions in the sol-gel process. In this manner, a polymeric network that can hold MNPs is created. [34]

2.3.3 hydrothermal method

Using the hydrothermal process, single crystals are created under high pressure and heat, depending on the solubility of the minerals. Hydrothermal synthesis is a practical technique for producing tiny particles. it has the benefits of a low energy need and a simple synthesis procedure. In hydrothermal synthesis, the powder materials are more pure because they begin with pure precursors.[35]

2.3.4 solvothermal method

The solvothermal process is a method used in materials science to synthesize materials, particularly nanomaterials, under high pressure and temperature conditions in a solvent. This process is typically carried out in a sealed vessel known as an autoclave. Solvothermal and hydrothermal are quite similar (where synesis conducted in a stainless steel autoclave), the only difference is the precursor solution usually not aqueous.

2.3.5 Spray pyrolysis method

Spray pyrolysis is a material processing technique used to create fine powder or thin film from a liquid precursor solution, where the constituents react to form a chemical compound. But the yield of the material lower. This method involves atomizing a liquid solution containing dissolved metal salts or organometallic compounds into fine droplets using a nozzle or nebulizer. The droplets are then transported by a carrier gas into a heated reaction zone, where they undergo pyrolysis (decomposition at high temperatures in the absence of oxygen) to form solid particles or a thin film on a substrate.

2.3.6 Co-precipitation method

Coprecipitation is when two or more particles are simultaneously precipitated from a solution. In this method, metal is deposited as a hydroxide from a salt precursor in the presence of a base in a solvent.

2.3.7 Carbothermal reduction method

Carbothermal reduction is a method used in metallurgy and materials science to make metals, alloys, and other materials. It involves heating metal oxides with carbon to produce the desired materials. First, the raw materials were mixed in the stoichiometric ratio. Then, they were ground together using ball milling in ethyl alcohol. After that, the mixture was heated in a tube furnace with argon gas.

CHAPTER 3:

CHARACTERISATION TECHNIQUES

3.1. X-Ray Diffraction (XRD)

X-ray diffraction (XRD) is a powerful analytical technique used to investigate the structure, composition, and properties of crystalline materials. Here's how XRD works and its applications:

Principle: When X-rays pass through a crystalline substance, the orderly and repeating pattern of atoms in the crystal structure causes the X-rays to interfere with each other. This interference can be either constructive, where the waves reinforce each other, or destructive, where the waves cancel each other out, depending on the specific arrangement of the atoms in the crystal lattice. This results in the scattering of X-rays in specific directions, producing a diffraction pattern. Angles and intensities of the diffracted X-rays are the two factors to analyse the crystal structure and lattice parameters.

Instrumentation: XRD apparatus usually includes three main components: a device that generate an X-ray, platform to hold the sample, and a detector. The X-ray source emits monochromatic X-rays, usually copper Kα radiation (λ = 1.5406 Å) or cobalt Kα radiation (λ = 1.78897 Å). The sample is mounted on a goniometer, which allows precise control of the angle of incidence and measurement of the diffraction angles. The X-ray intensity diffracted by the angle is recorded by the detector.

Data Analysis: by analysing the diffraction pattern by the interaction of X-rays with the sample, researchers can identify the specific crystalline phase present in the material, determine the arrangement of the atom within those phase(crystal structure) and the ascertain the preferred orientation of the crystals. This is typically done by comparing the experimental diffraction pattern with reference patterns from databases such as the International Centre for Diffraction Data (ICDD) or the Powder Diffraction File (PDF) [29].

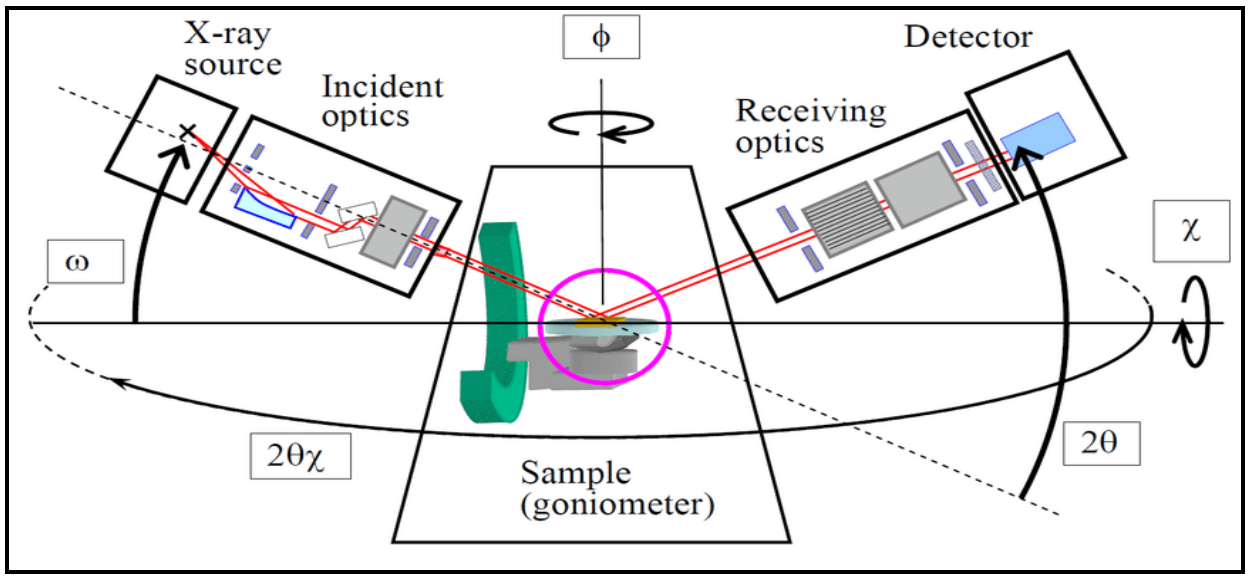

Figure 3.1 Schematic diagram of X-Ray Diffraction

3.2 Scanning Electron Microscopy (SEM)

Scanning Electron Microscopy (SEM) is a advance imaging method that allow us to observe and study the surface structure, shape and composition of the material with the exceptional detail and clarify, even at higher magnification. Here's a detailed explanation of how SEM works:

Principle of SEM: The principle behind SEM is scanning a sample's surface with a concentrated electron beam. Different signals arise when the electron beam interacts with the atoms in the sample; these signals include distinctive X-rays, backscattered electrons, and secondary electrons. The generated signals contain data that reveal the surface features and texture (topography), the types of elements present and their distribution (composition), and the arrangement of atoms in the crystalline regions (crystal structure) of the sample being analyzed.

Instrumentation: A SEM is made up of multiple key parts: an electron gun, electromagnetic lenses, a specimen chamber, detectors, and a computer system for image processing

The electron gun generates a finely focused beam of electrons, typically accelerated to energies ranging from a few kiloelectron volts (keV) to tens of kiloelectron volts.

Electromagnetic lenses focus and scan the electron beam across the surface of the sample with high precision.

Detectors collect various signals emitted by the sample, including secondary electrons (SE), backscattered electrons (BSE), and characteristic X-rays (EDS/EDX). The computer system processes the collected signals to generate high-resolution images and elemental maps of the sample's surface.

Imaging Modes:

Secondary Electron Imaging (SEI): SEI is the most commonly used imaging mode in SEM. It provides detailed topographical information about the sample's surface by detecting low-energy secondary electrons emitted from the top few nanometres of the specimen.

Backscattered Electron Imaging (BEI): BEI provides compositional contrast based on differences in atomic number (Z) between regions of the sample. Higher-Z materials produce more backscattered electrons, resulting in brighter areas in the image.

Elemental Mapping (EDS/EDX): Energy-dispersive X-ray spectroscopy (EDS or EDX) is often integrated with SEM to analyse the elemental composition of the sample. Elemental maps can be generated to visualize the distribution of specific elements across the sample's surface.

Sample Preparation: Sample preparation is crucial for SEM analysis and typically involves cleaning, drying, and coating the sample with a conductive layer (e.g., gold, palladium) to prevent charging effects and improve image quality. Non-conductive samples may require special treatment, such as sputter coating or carbon coating, to enhance conductivity and imaging quality [36].

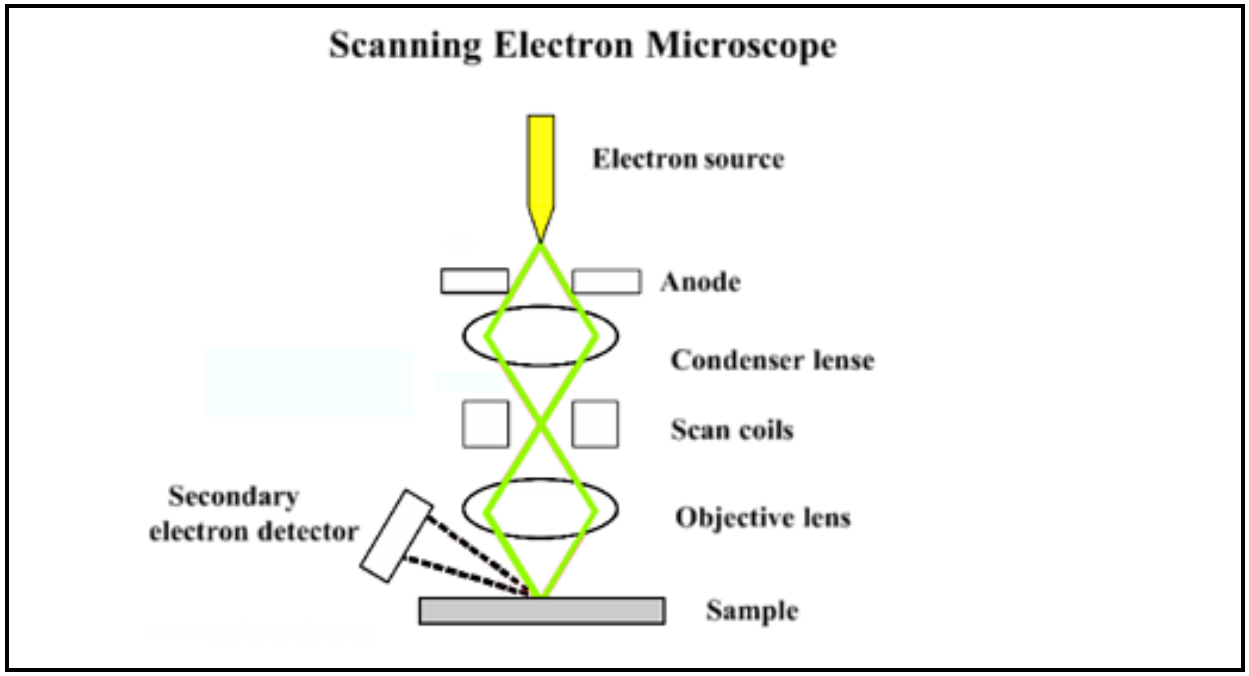

Figure 3.2 Schematic diagram of Scanning Electron Microscope (SEM)

3.3 Impedance spectroscopy

Principle of Impedance spectroscopy: Impedance spectroscopy is a powerful analytical technique used to measure the electrical impedance of a system over a range of frequencies.

The idea behind impedance spectroscopy is to measure the voltage response that occurs when an alternating current (AC) signal is applied to a sample. This answer gives information about the electrical characteristics of the sample, from which other physical and chemical aspects can be deduced.[37]

Instrumentation: To perform impedance spectroscopy, several key instruments are required.

Impedance Analyzer or LCR Meter: These instruments are specifically designed to measure impedance as a function of frequency. These techniques work by sending a low-intensity alternating current (AC) or voltage signal through the sample and then recording the corresponding voltage or current output, respectively.

Electrochemical Cell or Sample Holder: The sample under investigation is placed in an appropriate cell or holder. For solid samples, a two-electrode configuration is commonly used, with the sample sandwiched between the electrodes.

Potentiostat/Galvanostat: A potentiostat/galvanostat is a versatile instrument that can either regulate the voltage across a sample and measure the resulting current, or supply a controlled current to the sample and monitor the voltage response. Common in electrochemical impedance spectroscopy to control the electrochemical cell.

- Potentiostat: It measures the current by keeping constant voltage.
- Galvanostat: It measures the voltage by keeping constant current.

Computer with Control and Analysis Software: Controls the instrumentation, records the data, and performs the analysis. Specialized software packages for impedance spectroscopy are used for data acquisition, processing, and visualization (e.g., Nyquist plots, and Bode plots)

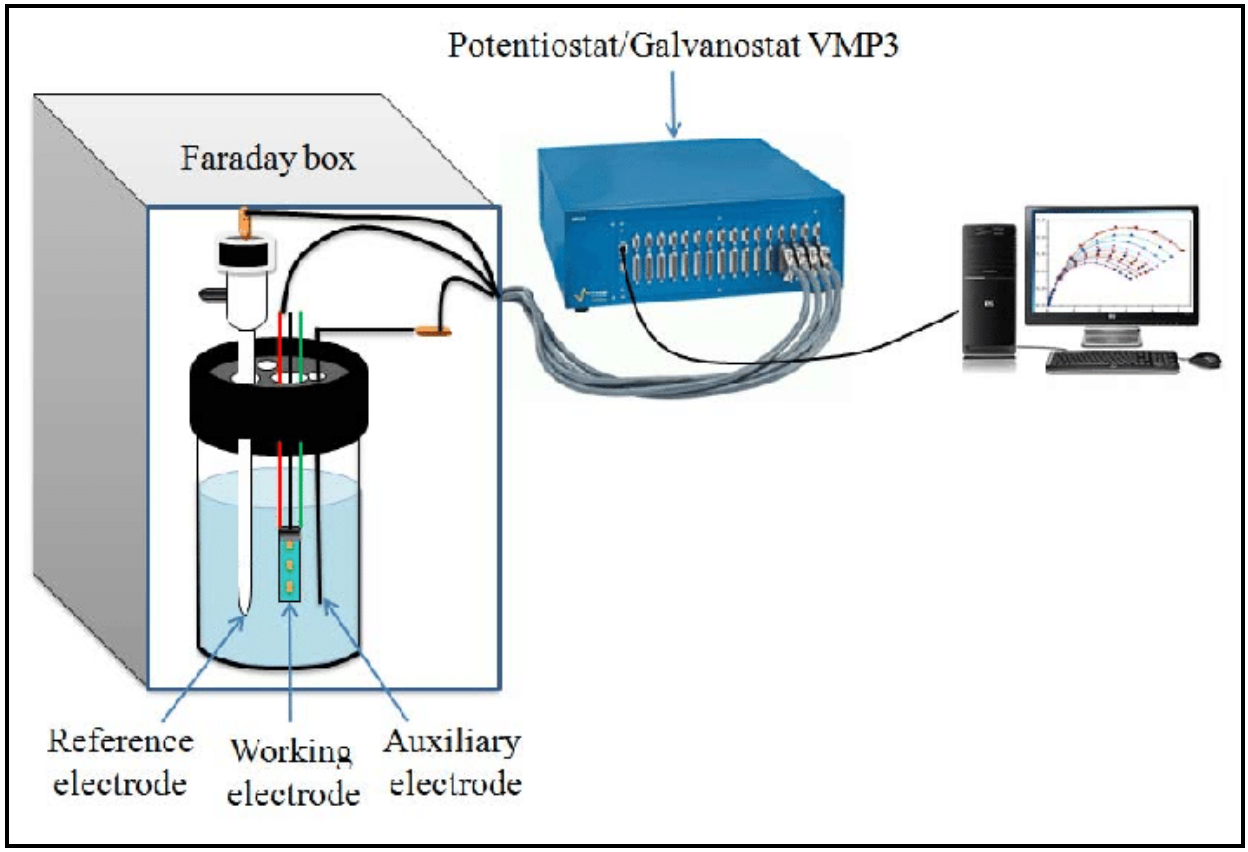

Figure 3.3 schematic diagram of impedance spectroscopy Set-up

Chapter 5

RESULTS AND DISCUSSION

4 Result and Discussion

4.1 Structural observations

The most widely used and conventional technique for producing $LiFePO_4$ involves solid-state reaction carried out in a reductive or inert environment to stop iron (II) from oxidizing into iron (III). However, because it calls for multiple high-temperature calcinations and grinding steps, this process takes a long time.

X-ray Diffraction (XRD) patterns of the $LiFePO_4$ cathode, synthesized through a solid-state reaction at different heating temperatures, as illustrated in Fig. 3. Graphs (a) and (b) show samples were first pre-heated at 300 °C, and then after grinding for 2h, they were calcinated at 700 °C shown in Graph (a) and at 750 °C shown in Graph (b). Likewise, graphs (c) and (d) show samples were pre-heated at 350 °C then after grinding for 2 h, they were calcinated at 700 °C shown in graph (c) and 750 °C shown in graph (d). the diffraction peak shown by XRD was quite narrow indicating they have a high degree of crystallinity. Compared with the JCPDS cards No. (40-1499) It was determined that every single diffraction peak in the samples belonged to the Pnma space group of the orthorhombic olivine phase structure of $LiFePO_4$ [18]. Out of four $LiFePO_4$ samples, graph (b) and graph (d) show the best resemblance compared to the standard $LiFePO_4$. And graph (b) and (d) both are calcinated at 750 °C. Graph (d) shows the excellent orthorhombic olivine phase of $LiFePO_4$ among the other three XRD which was synthesized at 350 °C and after 2h of grinding it was calcinated at 750 °C. For the formation of the olivine phase in the sample, calcination plays an important role. The diffraction peak induced by redox-active iron species is affected by calcination temperature in several ways. The identical structure ($LiFePO_4$) was obtained at 750°C i.e. graphs (b) and (d). The crystallinity of $LiFePO_4$ material is significantly influenced by the sintering temperature and carbon supply, as demonstrated by the XRD data. Complete crystallization occurred in the temperature range of 650–700 °C [20].

Scherrer's equation calculates the average crystal sizes of $LiFePO_4$. It is thus concluded that with the increase in synthesis temperature, the particle size grows and the crystallinity also increases [19]. All olivine compounds microcrystalline size (D_{XRD}) and average lattice strain (ε) were calculated using the Williamson-Hall equation (Eq. (1)) [26].

$$\beta_t \cos\theta = \varepsilon\,(4\sin\theta) + \frac{K\lambda}{D_{XRD}} \qquad (1)$$

where βt is the FWHM of XRD peaks or half-height width of the XRD diffraction peak; K is the dimensionless shape factor (0.9); Bragg angle is represented by θ; and λ stands for X-ray wavelength (Cu Ka, λ = 1.5406 Å). Kλ/D is the intercept on the y-axis.

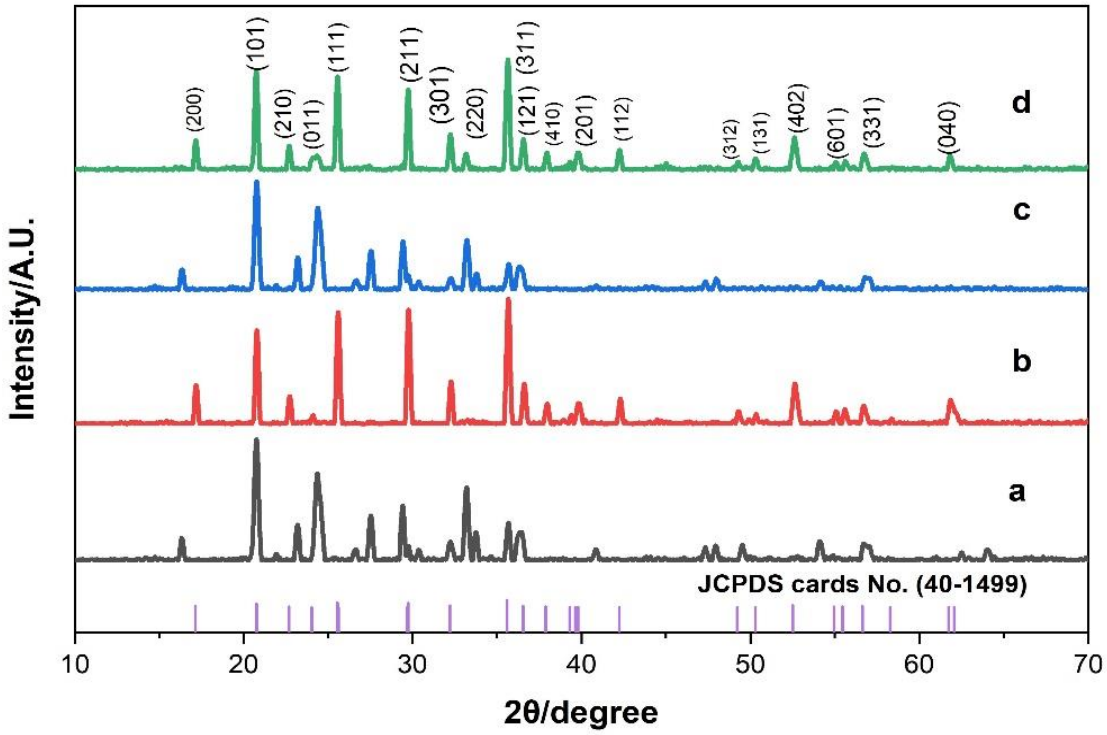

Fig. 4.1. XRD patterns of the $LiFePO_4$ cathode materials. The mixture was pre-heated in Ar/H_2 (90:10 v%) atmosphere (a), (b) at 300 °C for 12 h and (c), (d) at 350 °C. The resulting powder was ground again for 3 h and then calcinated (a), (c) at 700 °C and (b), (d) at 750 °C for 12 h under an Ar/H_2 (95:5 v%) atmosphere

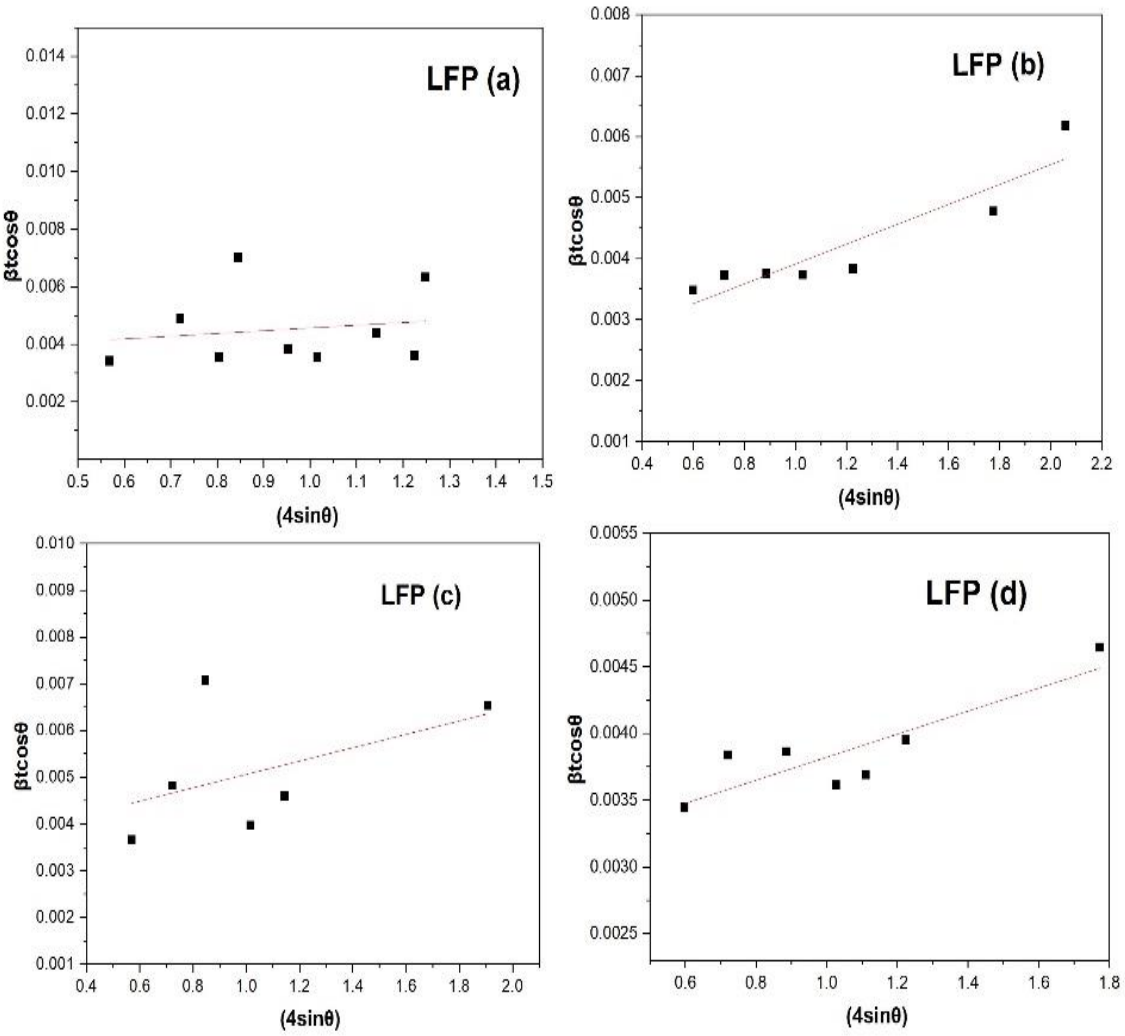

Fig. 4.2. W-H plot of LFP samples, graph between $\beta_t\cos\theta$ verses 4sinθ used to calculate strain.

According to the straight-line equation y = m x + c, using the W-H plot, βtcosθ vs (4sinθ) we calculated the strain in the different LFP samples(a)-(d). y= βtcosθ and x= (4sin θ).

The average crystallite size of different LFP samples is shown in Table 1. LFP (b) and (d) calcinated at 750 °C show slightly higher crystallite size compared to LFP (a) and (c) calcinated at 700 °C. Among all, LFP (d) preheated at 350 °C and calcinated at 750 °C shows higher crystallite size due to the agglomeration of the particles. The strain in the $LiFePO_4$ samples is shown by the W-H plot in Fig. 4. The lowest strain is shown by LFP (a) and (d).

Table 4.1. Crystallite or grain size and strain developed in different $LiFePO_4$ samples (a)-(d) synthesized under different temperatures.

$LiFePO_4$ XRD sample	Crystallite size D (nm)	Intercept/y	Slope/strain
LFP (a)	32.6794172	0.00362	$9.5*10^{-4}$
LFP (b)	34.08693753	0.00229	$1.6*10^{-3}$
LFP (c)	28.77340181	0.00636	$1.4*10^{-3}$
LFP (d)	36.16230881	0.00296	$8.6*10^{-4}$

4.2 Morphological observations

FE-SEM characterizes the surface morphology are shown in Fig. 4. (a)-(d) at different magnifications. irregular shapes and severe agglomeration are visible by the SEM image of $LiFePO_4$ appears to have sub-micrometer or micrometer sizes. We observed the particle size of the $LiFePO_4$ varying range between 500 nm and 10 μm. SEM images at different magnifications show highly porous structures and some spherical or rounded types of crystals visible under 5 μm particle size. In Figure 5(c), primary particles show agglomeration. It is well known that the morphology is quite complicated for particle synthesis by solid-state reaction because of the high heating temperatures, which generate unexpected aggregation and unusual particle shape.

Table 4.2. Elemental distribution by Weight % and Atomic% under 10 μm magnification in $LiFePO_4$ powder.

Element	Weight%	Atom%
Fe	46.7	22.8
P	16.6	14.6
O	36.7	62.5
Total	100.00	100.00

EDX elemental analysis of Fig. 4.3 confirms that particles in $LiFePO_4$ including Fe, P, O, and Li are present in the given sample with a certain atomic weight (%). As shown in Fig. 5 the EDX spectrum does not have an additional peak for any other element indicating that the $LiFePO_4$ sample is free of impurities. Sometimes due to the lighter nature of Li, Li element cannot be seen in the spectrum using EDX analysis [24]. Based on this analysis, we were able to determine the ratio of the elemental atoms, revealing O/Fe or O/P ratios of 4, and Fe/P ratio of 1. This verified the synthesis of the $LiFePO_4$ precursor [17].

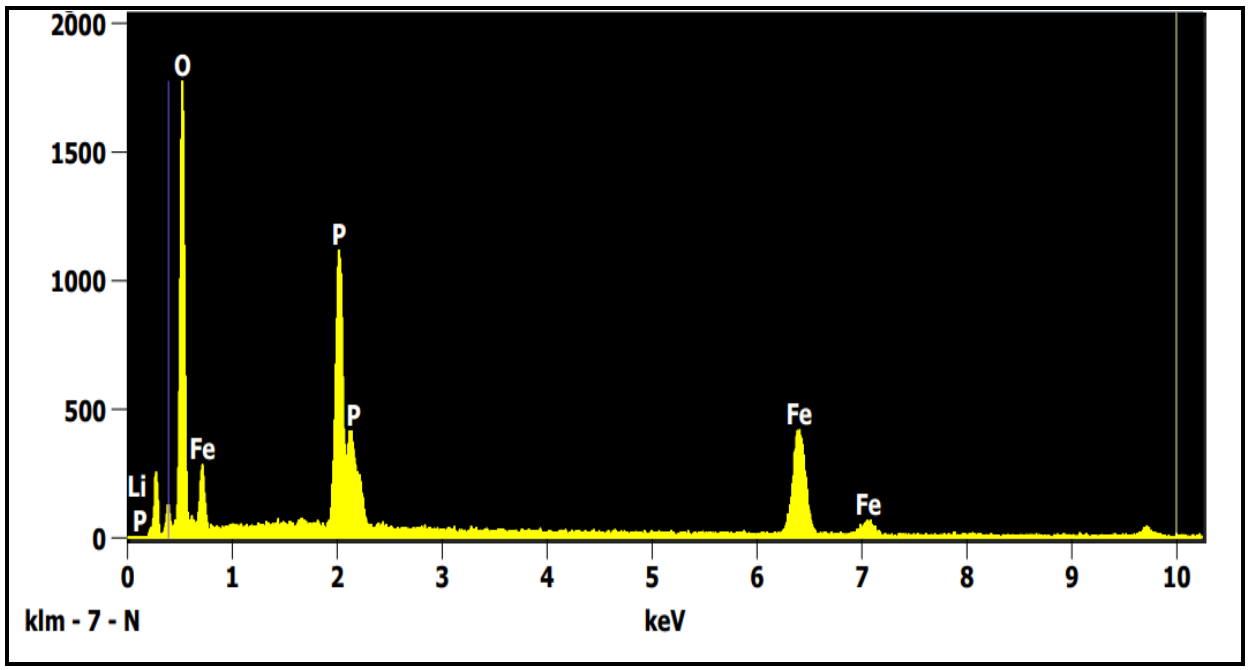

Fig. 4.3. EDX spectrum of $LiFePO_4$ powder sample

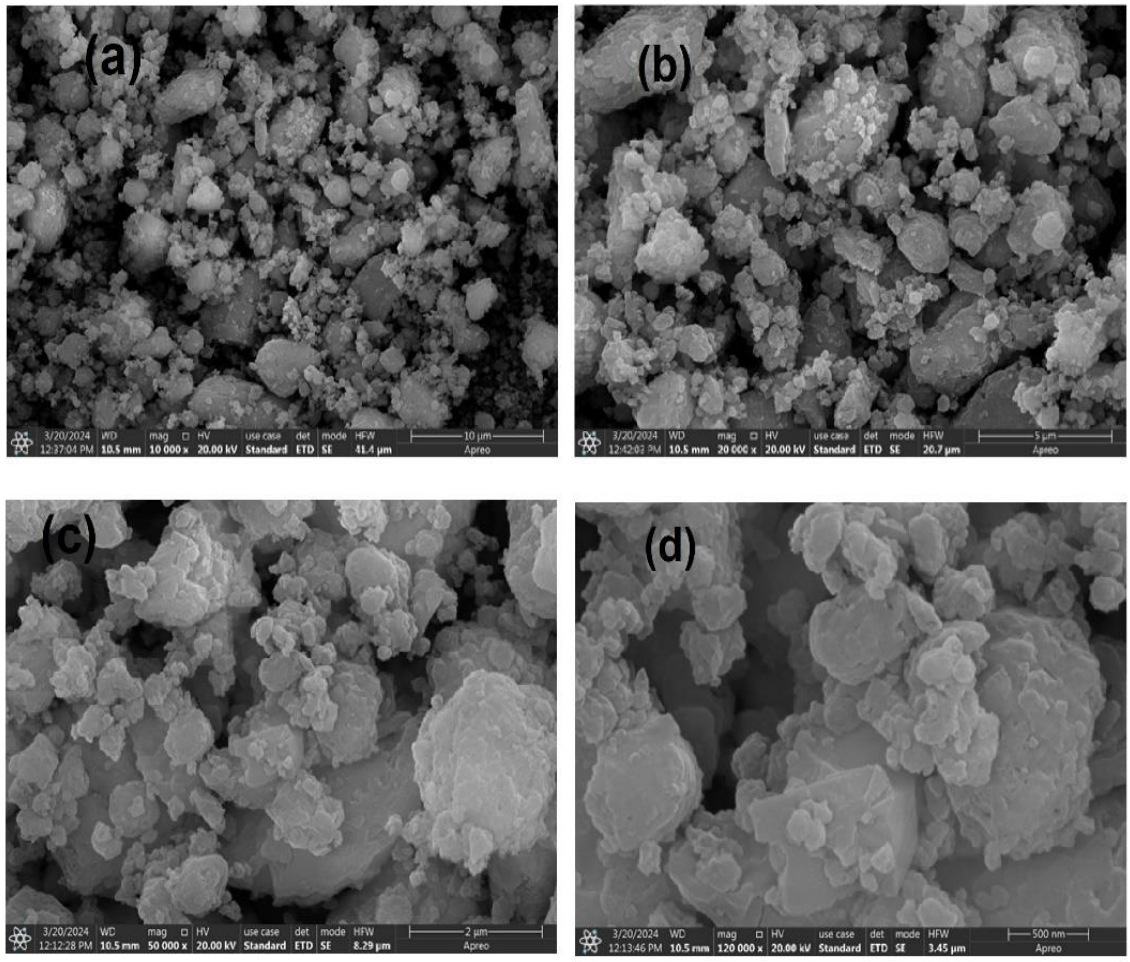

Fig. 4.4. (a) -(d) FE-SEM images of $LiFePO_4$ powder sample from 500 nm -10 µm

4.3 Dielectric analysis

The dielectric measurements provide valuable insights about the internal relaxation mechanism of the material including its dependence on temperature and frequency. The data obtained from these measurements provide valuable insights into two fundamental electrical properties of the material: dielectric loss, which represents the energy dissipation within the material, and electric permittivity (or dielectric constant), which describes the material's ability to store electrical energy shown in Fig. 7. The conduction and dielectric relaxation result in the dielectric loss inside the dielectric constant (εr) also known as relative permittivity relates to the amount of energy that a material can store in the form of charge under the influence of the applied electric field. When an alternating electric field is applied to a sample, the charge carriers within the material experience a

lag in their response to the changing field, resulting in a phenomenon called dielectric loss (D = tanδ). This delay in polarization causes energy to be dissipated as heat. The dielectric loss in the material is affected by two main factors: the flow of electric current (electrical conduction) and the time taken for the polarization to adjust to the changing field (dielectric relaxation).

The dielectric analysis of Fig. 7(a) shows that the dielectric constant value rises as the frequency increase. At lower frequencies, the dielectric constant decreases quickly, whereas at higher frequencies, it decreases gradually. The dielectric constant typically falls as frequency rises and becomes saturated at high frequencies. In the lower-frequency region, an initial rise in the dielectric spectra is caused by the collection of charge carriers close to the electrode. The dielectric constant decreases as the frequency rises because the dipoles can no longer rotate quickly as a result in no further ion diffusion occurs in the direction of the applied field because of the periodic reversal of the highly applied field. Hence, the dielectric constant value decreases with decrease in the accumulation of polarization-proliferated charge at the higher frequency region, so the field stops flowing, and polarization stops [25]. When the concentration of charge carriers rises results in an increase in the dielectric constant which in turn increases the conductivity of the sample. Comparing the dielectric constant at different temperatures from Fig. 7(a), the dielectric constant increases with an increase in temperature which increases the polarization. An increase in temperature induced in orientation results in a rise in the effective dipole, which raises the dielectric constant as well [38].

Fig. 7(b) shows the dielectric loss in $LiFePO_4$ samples. As a result of free charge motion occurring within the $LiFePO_4$ material, an increase in dielectric loss is observed at lower frequencies. These values, which result from the free charge in the material-electrode interface, influence the conductivity relaxation process rather than the bulk dielectric processes. [25]. It is also observed that the dielectric loss of $LiFePO_4$ samples decreases with an increase in frequency but up to some extent. The high significant dielectric loss can be attributed to the high resistivity of grain boundaries at a low frequency which are more effective than the grains. With an increase in temperature, permittivity loss is increased as shown in Fig. 7(b). But it also shows some of the permittivity loss that happens at a higher frequency may be due to the restriction by grain boundaries and the oscillating peak formed is also due to the transfer of maximum electrical energy into oscillating ions i.e. Fe^{2+} and Fe^{3+}. Since the grain boundary is

a high-resistance area, electron conduction will be restricted leading to space charge accumulation on grain boundaries generates space charge polarization [39].

4.4Impedance analysis

EIS is a valuable additional technique for evaluating the electrochemical behaviours of the electrode material. The cathode-electrolyte interface's charge transfer resistance can be determined using the EIS data. Higher charge transfer resistance is a sign of slower electrochemical kinetics, which may restrict the capacity of the battery and power output. In EIS analysis, the initial semicircle diameter is a crucial parameter for determining charge-transfer resistance. It is utilized to assess the charge transfer resistance of the formed systems, where a smaller impedance arc (DIA) diameter indicates lower charge transfer resistance.

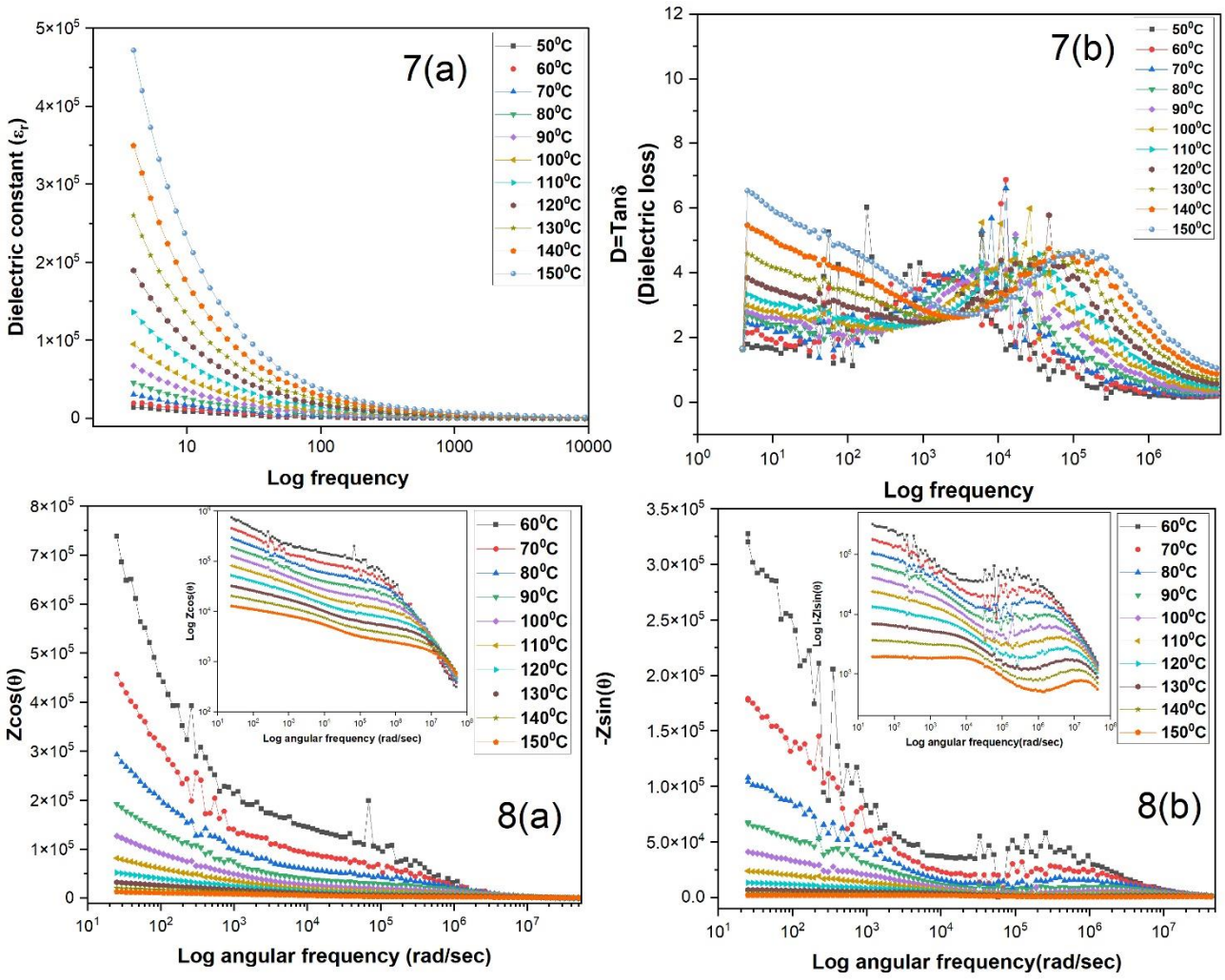

Fig. 4.7 . (a)Dielectric constant and (b) Dielectric loss variation with frequency at different temperature ranges (323-423K) for the $LiFePO_4$ sample.

Fig. 4.8. The real part/Zcosθ (a) and imaginary part/Zsinθ (b) of impedance measurement carried out at various temperatures (333-423K) across a frequency range of 4 Hz to 8 MHz for the $LiFePO_4$ sample.

$$Z' = |Z|\text{Cos}\theta \quad \text{and} \quad Z'' = |Z|\text{Sin}\theta \qquad (2)$$

here, |Z| represents the overall measured impedance, and θ denoted as phase angle measured in radians. Fig. 8 (a) and (b) illustrate how the real changes in the real and imaginary components of impedance varies with frequency at different temperatures within low frequency. The impedance measurements reveal that as the temperature increases, there is a corresponding reduction in impedance values. This inverse relationship between temperature and impedance indicates that the material has a negative temperature coefficient of resistance, meaning its electrical resistance decreases with rising temperatures. The impedance measurements show that the material exhibits higher resistance to the flow of electric current at low frequencies, but as the frequency of the applied alternating field increases, the impedance progressively diminishes, indicating that the material allows current to pass through more easily at higher frequencies. The decrease in impedance is because of the increased mobility with increasing frequency and release of immobile charges. With the increase in temperature, there is a decrease in barrier height resulting in the lowering of impedance. At higher frequencies, all of the curves merge because of the cancellation of the dipole orientation and the decrease in space charge [24,28].

The charge transfer resistance (R_{ct})for the $LiFePO_4$ decreases as the temperature increases, leading to a higher Li^+ ion diffusion coefficient. So high temperature is favorable for the reduction of resistivity and diffusion of more Li^+ ions in the $LiFePO_4$ samples.

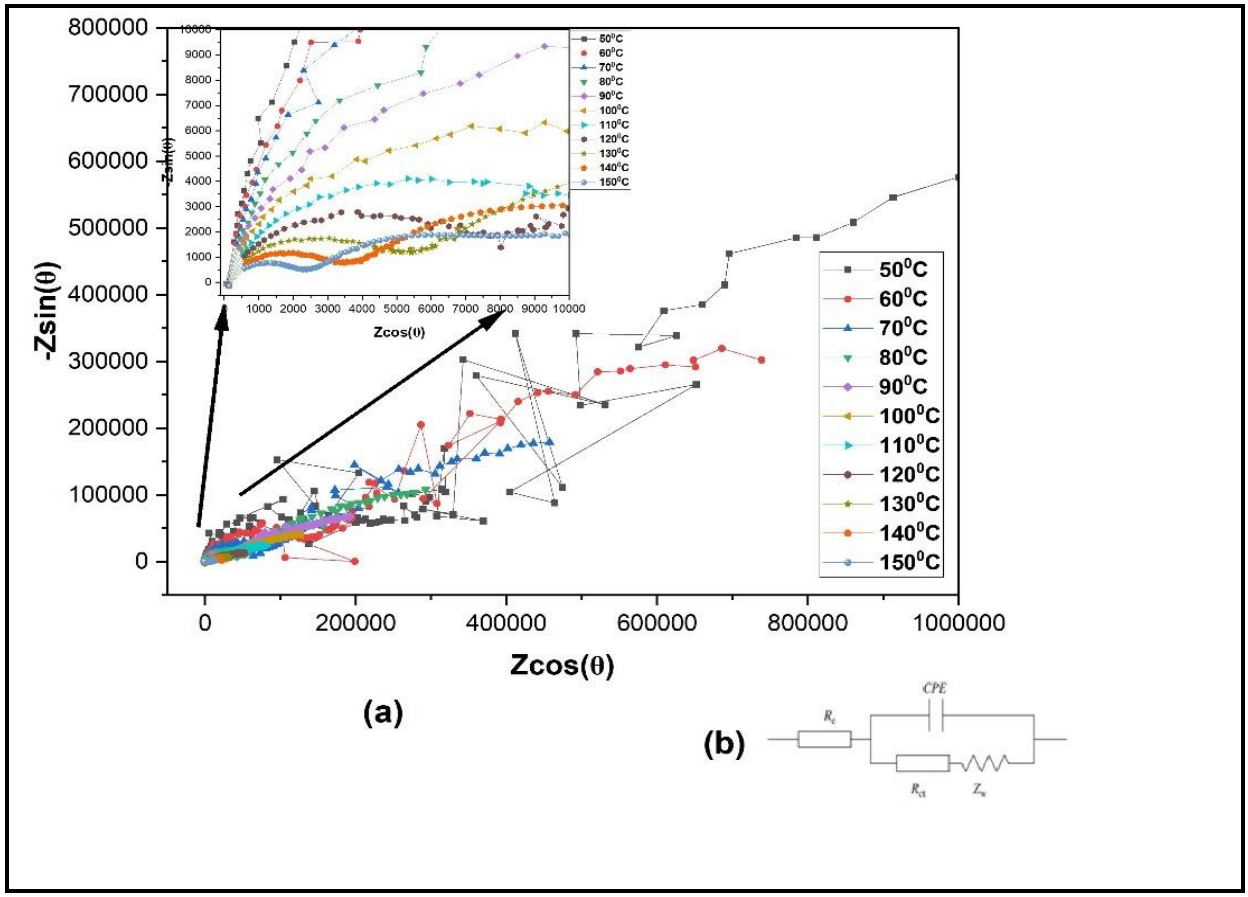

Fig. 4.9. (a) Nyquist plot of $LiFePO_4$ sample and (b) equivalent circuit model employed to fit the experimental EIS data.

Fig. 9 (a) shows the EIS result of $LiFePO_4$ at different temperatures (333-423K). charge transfer impedance (Rct) of the charged electrons moved from the electrode to the electrolyte is represented by the semi-circular portion of the high-frequency area of the graph. A decreased charge/transfer resistance is implied by a smaller impedance arc diameter (DIA). The DIA in Fig. 9 (a) is higher for lower temperatures and at higher temperatures the DIA is lower. This results in a lower value of charge/transfer resistance (R_{ct}) at higher temperatures. Also, the ohmic resistance (R_e), corresponding to the resistance of the electrolyte and electrode material, is related to an intercept at the Z' axis in high frequency. In addition, the low-frequency inclination line demonstrates the connection between the Warburg impedance (W_s) and Li^+ diffusion in LFP particles [40].

$$D_{Li+} = \frac{R^2T^2}{2A^2n^4C^2\sigma W^2} \qquad (3)$$

Here, n represents the number of electrons, T signifies the absolute temperature (298 K), R denotes the gas constant (8.314 J mol^{-1} K^{-1}), A represents surface area of cathode (cm^2), F is the Faraday constant (96,510 C mol^{-1}), C is associated with the Li^+ ions concentrations (mol L^{-1}), and σ_w represents the Warburg factor which correlates to $Z' = |Z|\cos\Theta$.

$$Z_{re} = R_e + R_{ct} + \sigma_w \omega^{-0.5} \quad (4)$$

In Eq. 3, R_e and R_{ct} represent the ohmic and charge transfer resistances (Ω) respectively, while ω denotes the angular frequency in low-frequency regions ($S^{-0.5}$) [42].

CHAPTER 6

CONCLUSION AND

FUTURE SCOPE

5 Conclusion

Pure LiFePO4 precursor was synthesized via solid-state reaction at varying calcination temperatures to determine the effect of the process. The olivine phase of LFP was crystallized in the Ar atmosphere at 600–800 °C. The products acquired were examined using XRD, FE-SEM, EDX, and EIS. The calcined olivine structure of $LiFePO_4$ at different temperatures was shown by the XRD result. FE-SEM results showed that $LiFePO_4$ morphology. Agglomeration is visible and large particles is also present. The best XRD result resembled the $LiFePO_4$ (d) preheated at 350 °C and calcinated at 750 °C of 36 nm crystallite size with lower strain around $8.6*10^{-4}$. EDX data showed the elemental distribution in the bare $LiFePO_4$ and the impurity peak is also absent showed by EDX. EIS result showed the impedance and dielectric properties of pure $LiFePO_4$. In the dielectric study, the $LiFePO_4$ sample showed high permittivity and polarization at higher temperatures and lower frequency of applied field, relaxation in permittivity is also observed at higher temperatures for pure $LiFePO_4$ and showed oscillating peak. In the impedance study, the $LiFePO_4$ sample showed lower charge/transfer resistance (Rct) at higher temperatures under high-frequency reasons that resulted in a more diffusion of Li^+ ion.

Future scope:

The future scope of $LiFePO_4$ (LFP) batteries is promising due to their excellent safety, stability, and environmental friendliness. Some potential areas for future research and development include: Improving energy density, Incorporating nanostructured LFP materials can improve the battery's rate capability, cycling stability, and overall performance, Doping LFP with other elements or modifying its surface can enhance its electrochemical properties, such as electronic conductivity and lithium-ion diffusion, Developing novel electrolyte formulations that are stable at higher voltages and temperatures can extend the life and performance of LFP batteries, Developing efficient recycling processes for LFP batteries and exploring their potential for second-life applications, such as grid storage, can reduce environmental impact and enhance the overall sustainability of the technology, Combining LFP batteries with other energy storage technologies, such as supercapacitors or fuel cells, can create high-performance hybrid systems for specific applications.

As research continues to address these challenges and opportunities, LFP batteries are likely to play an increasingly important role in the transition towards sustainable energy storage solutions.

CHAPTER 7

REFERENCES

References

1. Terada, N., Yanagi, T., Arai, S., Yoshikawa, M., Ohta, K., Nakajima, N., Yanai, A. and Arai, N., 2001. Development of lithium batteries for energy storage and EV applications. *Journal of Power Sources*, *100*(1-2), pp.80-92.
2. Andersson, A.S., Kalska, B., Häggström, L. and Thomas, J.O., 2000. Lithium extraction/insertion in LiFePO4: an X-ray diffraction and Mössbauer spectroscopy study. *Solid State Ionics*, *130*(1-2), pp.41-52.
3. Mizushima, K.J.P.C., Jones, P.C., Wiseman, P.J. and Goodenough, J.B., 1980. LixCoO2 (0< x<-1): A new cathode material for batteries of high energy density. *Materials Research Bulletin*, *15*(6), pp.783-789.
4. Zhang, W.J., 2011. Structure and performance of LiFePO4 cathode materials: A review. *Journal of Power Sources*, *196*(6), pp.2962-2970.
5. Phospho-olivines as Positive-Electrode Materials for Rechargeable Lithium Batteries--DOI (10.1149/1.1837571)
6. Ellis, B.L., Lee, K.T. and Nazar, L.F., 2010. Positive electrode materials for Li-ion and Li-batteries. *Chemistry of materials*, *22*(3), pp.691-714M. Takahashi, S. Tobishima, K. Takei, Y. Sakurai, Solid State Ionics 148 (2002) 283.
7. Xu, Z., Gao, L., Liu, Y. and Li, L., 2016. recent developments in the doped LiFePO4 cathode materials for power lithium ion batteries. *Journal of the Electrochemical Society*, *163*(13), p.A2600.
8. A.K. Padhi, K.S. Nanjundaswamy, J.B. Goodenough, Journal of Electrochemical Society 144 (1997) 1188.
9. M. S. Islam, D. J. Driscoll, C. A. J. Fisher, and P. R. Slater, Chemistry of Materials, 17(20), 5085 (2005).
10. M.S. Islam, D.J. Driscoll, C.A.J. Fisher, P.R. Slater, Chemistry of Materials 17 (2005) 5085.
11. Saroha, R., Panwar, A.K., Sharma, Y., Tyagi, P.K. and Ghosh, S., 2017. Development of surface functionalized ZnO-doped LiFePO4/C composites as alternative cathode material for lithium ion batteries. *Applied Surface Science*, *394*, pp.25-36.
12. Zhang, Yong, et al. "Advances in new cathode material LiFePO4 for lithium-ion batteries." *Synthetic Metals* 162.13-14 (2012): 1315-1326.

13. Zhang, S.S., Allen, J.L., Xu, K. and Jow, T.R., 2005. Optimization of reaction condition for solid-state synthesis of LiFePO4-C composite cathodes. *Journal of Power Sources*, *147*(1-2), pp.234-240.
14. Andersson, A.S., Kalska, B., Häggström, L. and Thomas, J.O., 2000. Lithium extraction/insertion in LiFePO4: an X-ray diffraction and Mössbauer spectroscopy study. *Solid State Ionics*, *130*(1-2), pp.41-52.
15. Whittingham, M.S., 2004. Lithium batteries and cathode materials. *Chemical reviews*, *104*(10), pp.4271-4302.
16. Lyczko, N., Nzihou, A., Sharrock, P., Germeau, A. and Toussaint, C., 2012. Characterization of LiFePO4/C cathode for lithium ion batteries. *Industrial & engineering chemistry research*, *51*(1), pp.292-300.
17. Scrosati, B., Abraham, K.M., van Schalkwijk, W.A. and Hassoun, J. eds., 2013. *Lithium batteries: advanced technologies and applications*. John Wiley & Sons.
18. Chen, Z.Y., Zhu, H.L., Ji, S., Fakir, R. and Linkov, V., 2008. Influence of carbon sources on electrochemical performances of LiFePO4/C composites. *Solid State Ionics*, *179*(27-32), pp.1810-1815.
19. Yamada, A., Chung, S.C. and Hinokuma, K., 2001. Optimized LiFePO4 for lithium battery cathodes. *Journal of the Electrochemical Society*, *148*(3), p.A224.
20. Zhang, Y., Huo, Q.Y., Du, P.P., Wang, L.Z., Zhang, A.Q., Song, Y.H., Lv, Y. and Li, G.Y., 2012. Advances in new cathode material LiFePO4 for lithium-ion batteries. *Synthetic Metals*, *162*(13-14), pp.1315-1326.
21. Nguyen, T.H., Fraiwan, A. and Choi, S., 2014. based batteries: A review. *Biosensors and Bioelectronics*, *54*, pp.640-649.Abe, Y., Hori, N. and Kumagai, S., 2019. Electrochemical impedance spectroscopy on the performance degradation of LiFePO4/graphite lithium-ion battery due to charge-discharge cycling under different C-rates. *Energies*, *12*(23), p.4507.
22. Lisbona, D. and Snee, T., 2011. A review of hazards associated with primary lithium and lithium-ion batteries. *Process safety and environmental protection*, *89*(6), pp.434-442.Abhilash, K.P., Selvin, P.C., Nalini, B., Xia, H., Adams, S. and Reddy, M.V., 2018. Electrochemical analysis of the carbon-encapsulated lithium iron phosphate nanochains and their high-temperature conductivity profiles. *ACS omega*, *3*(6), pp.6446-6455.
23. Hosen, M.S., Gopalakrishnan, R., Kalogiannis, T., Jaguemont, J., Van Mierlo, J. and Berecibar, M., 2021. Impact of relaxation time on EIS characterization of the lithium battery technologies—experimental study and chemistry-neutral modelling. *World Electric Vehicle Journal*, *12*(2), p.77.

24. Y. Liu, Y.-J. Gu, G.-Y. Luo, Z.-L. Chen, F.-Z. Wu, X.-Y. Dai, Y. Mai, J.-Q. Li, Ni-doped LiFePO4/C as high-performance cathode composites for Li-ion batteries, Ceram. Int. 46 (10) (2020) 14857–14863.
25. Kumar, R.V. and Sarakonsri, T., 2010. A review of materials and chemistry for secondary batteries. *High Energy Density Lithium Batteries: Materials, Engineering, Applications*, pp.53-80.
26. Marin-Garcia, G., Vazquez-Guzman, G., Sosa, J.M., Lopez, A.R., Martinez-Rodriguez, P.R. and Langarica, D., 2020, November. Battery types and electrical models: A review. In *2020 IEEE International Autumn Meeting on Power, Electronics and Computing (ROPEC)* (Vol. 4, pp. 1-6). IEEE.
27. Priyono, B., et al., Synthesis of lithium titanate (Li4Ti5O12) through hydrothermal process by using lithium hydroxide (LiOH) and titanium dioxide (TiO2) xerogel. International Journal of Technology, 2015. 6(4): p. 555-564.
28. Sofyan, N., et al., Effect of Different Calcination Temperatures and Carbon Coating on the Characteristics of LiFePO4 Prepared by Hydrothermal Route. Int. J. Eng. Technol, 2017. 9(4): p. 3310-3317
29. Mekonnen, Y., Sundararajan, A. and Sarwat, A.I., 2016. A review of cathode and anode materials for lithium-ion batteries. *SoutheastCon 2016*, pp.1-6.
30. Eriksson, T., 2001. *LiMn2O4 as a Li-Ion battery cathode. From bulk to electrolyte interface* (Doctoral dissertation, Acta Universitatis Upsaliensis).
31. Tripathi, R., Gardiner, G.R., Islam, M.S. and Nazar, L.F., 2011. Alkali-ion conduction paths in LiFeSO4F and NaFeSO4F tavorite-type cathode materials. *Chemistry of Materials*, *23*(8), pp.2278-2284.
32. Ramesh, T.N., Lee, K.T., Ellis, B.L. and Nazar, L.F., 2010. Tavorite lithium iron fluorophosphate cathode materials: phase transition and electrochemistry of LiFePO4F–Li2FePO4F. *Electrochemical and Solid-State Letters*, *13*(4), p.A43
33. Gim, J., Song, J., Nguyen, D., Alfaruqi, M.H., Kim, S., Kang, J., Rai, A.K., Mathew, V. and Kim, J., 2014. A two-step solid state synthesis of LiFePO4/C cathode with varying carbon contents for Li-ion batteries. *Ceramics International*, *40*(1), pp.1561-1567.
34. Yilmaz, E. and Soylak, M., 2020. Functionalized nanomaterials for sample preparation methods. In *Handbook of Nanomaterials in analytical chemistry* (pp. 375-413). Elsevier.
35. Chen, J., Wang, S. and Whittingham, M.S., 2007. Hydrothermal synthesis of cathode materials. *Journal of Power Sources*, *174*(2), pp.442-448.
36. Ngo, D.T., Scipioni, R., Simonsen, S.B., Jørgensen, P.S. and Jensen, S.H., 2016. A TEM study of morphological and structural degradation phenomena in LiFePO4-CB cathodes. *International Journal of Energy Research*, *40*(14), pp.2022-2032.

37. Portalis, G., Carrapa, E., Simon, B. and Vivier, V., 2021. Electrochemical impedance spectroscopy investigation on battery materials using a symmetrical cell. *Journal of Solid State Electrochemistry*, *25*(6), pp.1915-1926.
38. Meena, R. and Dhaka, R.S., 2022. Dielectric properties and impedance spectroscopy of NASICON type Na3Zr2Si2PO12. *Ceramics International*, *48*(23), pp.35150-35159.
39. Guo, Y., Zhu, J. and Li, H., 2021. Structure, electromagnetic and dielectric properties of Ti-substituted lithium--zinc ferrite. *Journal of Materials Science: Materials in Electronics*, *32*, pp.8354-8365.
40. Jin, B., Jin, E.M., Park, K.H. and Gu, H.B., 2008. Electrochemical properties of LiFePO4-multiwalled carbon nanotubes composite cathode materials for lithium polymer battery. *Electrochemistry Communications*, *10*(10), pp.1537-1540.
41. Jin, B., Jin, E.M., Park, K.H. and Gu, H.B., 2008. Electrochemical properties of LiFePO4-multiwalled carbon nanotubes composite cathode materials for lithium polymer battery. *Electrochemistry Communications*, *10*(10), pp.1537-1540.
42. Zou, G., Chen, K., Luo, X., Fu, Q. and Wu, B., 2024. Crystal structure, morphology, and electrical properties of aluminum-doped LFP materials. *Ionics*, pp.1-15.

CERTIFICATE:

ICAMNOP - 2023

International Conference on
Atomic, Molecular, Material, Nano, and Optical Physics with Applications

20th - 22nd December, 2023

Organized by:
Department of Applied Physics, Delhi Technological University, Delhi, India

Certificate

This is to certify that

Prof./Dr./Mr./Ms. Ankit Chaturvedi

has presented Poster / Oral Presentation in the **"International Conference on Atomic, Molecular, Material, Nano and Optical Physics with Applications (ICAMNOP-2023)"** held at Delhi Technological University, Delhi, India during 20th-22nd December, 2023.

Prof. Rinku Sharma
President, ICAMNOP-2023

Prof. A. S. Rao
Chairperson, ICAMNOP-2023

Prof. Vinod Singh
Convener, ICAMNOP-2023

PAPER NAME

ankit thesis.docx

WORD COUNT

9779 Words

CHARACTER COUNT

56383 Characters

PAGE COUNT

55 Pages

FILE SIZE

2.8MB

SUBMISSION DATE

Jun 5, 2024 5:46 PM GMT+5:30

REPORT DATE

Jun 5, 2024 5:47 PM GMT+5:30

10% Overall Similarity

The combined total of all matches, including overlapping sources, for each database.

- 6% Internet database
- 4% Publications database
- Crossref database
- Crossref Posted Content database
- 7% Submitted Works database

Excluded from Similarity Report

- Bibliographic material
- Quoted material
- Cited material
- Small Matches (Less then 10 words)
- Manually excluded text blocks

10% Overall Similarity

Top sources found in the following databases:

- 6% Internet database
- Crossref database
- 7% Submitted Works database
- 4% Publications database
- Crossref Posted Content database

TOP SOURCES

The sources with the highest number of matches within the submission. Overlapping sources will not be displayed.

1	dspace.dtu.ac.in:8080 Internet	<1%
2	Delhi Technological University on 2024-05-23 Submitted works	<1%
3	University of Dundee on 2024-04-28 Submitted works	<1%
4	repositories.lib.utexas.edu Internet	<1%
5	omicsonline.org Internet	<1%
6	Atlantic Technological University on 2023-06-21 Submitted works	<1%
7	Jihyeon Gim, Jinju Song, Diem Nguyen, Muhammad Hilmy Alfaruqi et a... Crossref	<1%
8	National Institute of Technology, Raipur on 2024-06-05 Submitted works	<1%

9	UC, San Diego on 2024-04-27 Submitted works	<1%
10	Jing Geng, Zhengguang Zou, Tianxing Wang, Shuchao Zhang, Shenglin... Crossref	<1%
11	Springfield Central State High School on 2023-08-30 Submitted works	<1%
12	De Montfort University on 2022-06-05 Submitted works	<1%
13	Georgia Institute of Technology on 2009-03-24 Submitted works	<1%
14	University of the Free State on 2024-05-30 Submitted works	<1%
15	Wei-Jun Zhang. "Structure and performance of LiFePO4 cathode mater... Crossref	<1%
16	www2.mdpi.com Internet	<1%
17	Mikael Mollazadeh, Biuck Habibi. "LiFePO4/Carbon/Reduced Graphene... Crossref	<1%
18	Ramcharan Meena, Rajendra S. Dhaka. "Dielectric properties and impe... Crossref	<1%
19	dalspace.library.dal.ca Internet	<1%
20	dspace.ncl.res.in:8080 Internet	<1%

21	link.springer.com Internet	<1%
22	vjol.info.vn Internet	<1%
23	University of Wollongong on 2021-06-04 Submitted works	<1%
24	jbcs.sbq.org.br Internet	<1%
25	Khalifa University of Science Technology and Research on 2020-11-21 Submitted works	<1%
26	University of Bradford on 2023-07-31 Submitted works	<1%
27	dipot.ulb.ac.be Internet	<1%
28	iopscience.iop.org Internet	<1%
29	papyrus.bib.umontreal.ca Internet	<1%
30	ijee.net Internet	<1%
31	Bin Huang, Suqin Liu, Hongliang Li, Shuxin Zhuang, Dong Fang. " Comp... Crossref	<1%
32	University of St Andrews on 2023-07-27 Submitted works	<1%

33	Yong Zhang, Qing-yuan Huo, Pei-pei Du, Li-zhen Wang, Ai-qin Zhang, Y... Crossref	<1%
34	hdl.handle.net Internet	<1%
35	oak.go.kr Internet	<1%
36	voltagenote.com Internet	<1%
37	Chandigarh Group of Colleges on 2023-11-22 Submitted works	<1%
38	Km. Komal, Mukhtiyar Singh, Bharti Singh. "Effect of rGO weight perce... Crossref	<1%
39	Nanyang Technological University, Singapore on 2013-04-20 Submitted works	<1%
40	Napier University on 2023-08-22 Submitted works	<1%
41	Polytechnic of Turin on 2022-06-07 Submitted works	<1%
42	University of Wales Swansea on 2018-05-23 Submitted works	<1%
43	Zhaofeng Liu, Guodong Du, Yingke Zhou, Xiaohui Tian. "Freeze-casting ... Crossref	<1%
44	pluginhighway.ca Internet	<1%

45	nmletters.org Internet	<1%
46	De Montfort University on 2023-09-17 Submitted works	<1%
47	Gui-Yang Luo, Yi-Jing Gu, Yuan Liu, Zi-Liang Chen, Yong-lin Huo, Fu-Zh... Crossref	<1%
48	Higher Education Commission Pakistan on 2014-03-13 Submitted works	<1%
49	Napier University on 2024-05-29 Submitted works	<1%
50	RMIT University on 2020-03-14 Submitted works	<1%
51	Savitribai Phule Pune University on 2018-05-08 Submitted works	<1%
52	University of Sheffield on 2019-04-29 Submitted works	<1%
53	University of Sydney on 2024-05-02 Submitted works	<1%
54	nccur.lib.nccu.edu.tw Internet	<1%
55	repository.lib.ncsu.edu Internet	<1%
56	vdoc.pub Internet	<1%

Excluded from Similarity Report

- Bibliographic material
- Cited material
- Manually excluded text blocks
- Quoted material
- Small Matches (Less then 10 words)

EXCLUDED TEXT BLOCKS

Department of Applied PhysicsDELHI TECHNOLOGICAL UNIVERSITY(formerly Del...

dspace.dtu.ac.in:8080

A Project

Loughborough University on 2021-09-03

has not been

dtusimilarity on 2024-05-29

DELHI TECHNOLOGICAL UNIVERSITY(formerly Delhi College of Engineering)Shah...

Delhi Technological University on 2024-05-23

not form the

Delhi Technological University on 2024-05-23

Delhi Technological University

dspace.dtu.ac.in:8080

to express my gratitude towards my project supervisor, Prof. Rajinder. K. Gupta,De...

dspace.dtu.ac.in:8080

anorthorhombic

link.springer.com

Introduction andLiterature Review

ir.jkuat.ac.ke

Paper 044

Submit New Version

Title Structural, Morphological, Dielectric and Impedance Study of Lithium Iron Phosphate (LiFePO4)
Submitted April 12, 2024 to ICAMNOP-2023
Status 1st revision
History 3 previous version(s)

Authors

Contact Authors

AC Ankit chaturvedi

AP Amrish Panwar
Delhi technological university
amrishphy@dtu.ac.in

RG Rajinder Gupta
Delhi technological university
rkg67ap@yahoo.com

Abstract

Lithium-ion batteries are getting more attention as prominent energy storage devices because of their high-power energy density and better cyclability compared to other energy storage devices. With the growing interest in developing rechargeable batteries, For the next generation of Li-ion batteries, lithium iron phosphate (LiFePO4) is one of the potential cathode materials because of its more cyclic stability, environmental friendliness and economic viability. Here in this study, The LiFePO4 cathode material has been synthesized using a solid-state reaction method using two-step heating under different calcination temperatures in a reduced inert atmosphere. Pre-heating results in decomposition and calcination at high temperatures leading to the crystallization of LiFePO4. Primary LiFePO4 was synthesized by preheating at 350 0C and calcinated at 750 0C. The structural, morphology, elemental distribution and Impedance with Dielectric study of synthesized pristine LiFePO4 are carried out by X-ray powder diffraction (XRD), Field emission Scanning electron microscopy (FE-SEM), and electrochemical impedance spectroscopy (EIS), respectively. XRD result

Reports

For this latest paper version:

Report

Make the abstract more brief
Re-check the subscript and super script in chemical formula for many compounds.
Explain stoichiometric proportions in synthetic method
Why temperature of 700 or 750 oC selected?
Use multiplication sign from symbol in Table 1 last column
Check figure 5 and 6, and their explanation in text, need correction

PDF

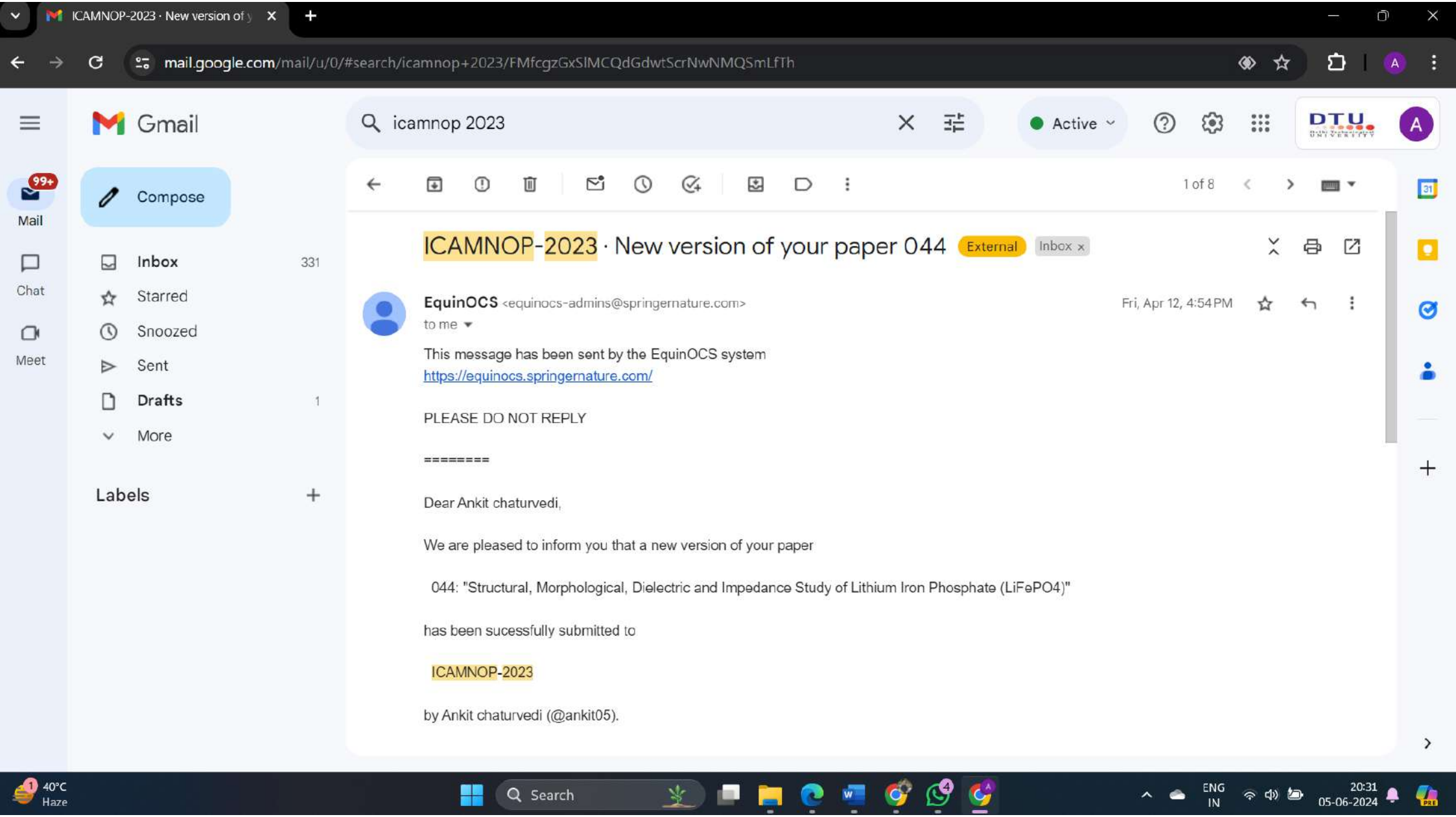
ICAMNOP-2023 · New version of y
mail.google.com/mail/u/0/#search/icamnop+2023/FMfcgzGxSlMCQdGdwtScrNwNMQSmLfTh
Gmail
icamnop 2023
Active
Compose
Inbox 331
Starred
Snoozed
Sent
Drafts 1
More
Labels
Mail
Chat
Meet
1 of 8
ICAMNOP-2023 · New version of your paper 044
External
Inbox ×
EquinOCS <equinocs-admins@springernature.com>
Fri, Apr 12, 4:54 PM
to me
This message has been sent by the EquinOCS system
https://equinocs.springernature.com/
PLEASE DO NOT REPLY
========
Dear Ankit chaturvedi,
We are pleased to inform you that a new version of your paper
044: "Structural, Morphological, Dielectric and Impedance Study of Lithium Iron Phosphate (LiFePO4)"
has been sucessfully submitted to
ICAMNOP-2023
by Ankit chaturvedi (@ankit05).
40°C
Haze
Search
ENG
IN
20:31
05-06-2024